Chapter-5

INSIGHT INTO THE STRUCTURAL REQUIREMENT OF CYTOCHROME P450 LANOSTEROL 14α -DEMETHYLASE INHIBITORS BASED ON 3D-QSAR AND MOLECULAR DOCKING

5.1 Abstract

To investigate the structural requirements of Cytochrome P450 lanosterol 14α-demethylase (CYP51) inhibition for the series of triazole derivatives as antifungal agents, a three-dimensional quantitative structure activity relationship (3D-QSAR) using comparative molecular field analysis (CoMFA) and comparative molecular similarity indices analysis (CoMSIA) methods were performed. Assessment of 24 compounds as training set served to set up model, while it was validated by assessment of a set of 9 test set compounds. Most potent molecule with least energy conformer obtained from the systematic search was used as a template structure for the alignment of the data set. The optimum partial least squares (PLS) for CoMFA and CoMSIA models illustrated good 'leave-one-out' cross-validated coefficient (q2) of 0.611 and 0.792, the coefficient of determination (r2) of 0.982 and 0.953 and good predicted power (r2pred) of 0.871 and 0.752 respectively. Docking results showed that those compounds which have capability to interact with heme group could possess high inhibitory activity. The final models of QSAR along with information gathered from contour maps and docking study may be used for designing of novel analogs as potential antifungal agents.

5.2 Introduction

Life-threatening fungal infections have increased dramatically in immune compromised patients caused by pathogenic fungi are becoming increasingly common, especially in those individuals who undergo organ transplants, patients with Acquired Immuno Deficiency Syndrome and tumors.[1-4]

Fungal infections remain a significant cause of morbidity and mortality. Antifungal drugs discovery has identified three classes of natural products (griseofulvin, polyenes and echinocandins) and four classes of synthetic chemicals (azoles, allylamines, flucytosine and phenyl morpholines) with great clinical value against fungal infections.[5-11] Clinically candidosis, aspergillosis and cryptococcosisare are three major fungal infections in

immune compromised individuals. The major opportunistic pathogen has been Candida albicans. The management of invasive fungal infection utilizes a variable multidisciplinary approach involving antifungals, appropriate surgery an immuno-correction. Currently available antifungal drugs have essentially three molecular targets: sterol 14α-demethylase (azoles), ergosterol (polyenes) and β-1, 3-glucan synthetase (echinocandins). Azole antifungals interfere with cell membrane ergosterol synthesis via inhibition of cytochrome P450 14α-sterol demethylase enzyme.[12, 13] The natural substrate, lanosterol is prevented through binding of the azole ring to the iron of porphyrin.[14] Azole antifungal drugs block the biosynthesis of fungal cell membranes and suppress fungal growth by inhibiting CYP51 which is a critical enzyme in the ergosterol synthesis pathway.[15]

Azole antifungal drugs are widely used in clinical treatment[16]; in particular, Fluconazole, Itraconazole, Voriconazole, posaconazole etc.[17, 18] However, the extensive use of azole antifungal drugs has led to the resistance of clinical pathogenic fungi to drug treatment; one of the main causes of clinical treatment failure.[19] Therefore, development of new azole drugs for clinical treatment is a pressing need.

Limitations in their clinical applications include a narrow spectrum (fluconazole), variable bioavailability (itraconazole), drug interactions, e.g. with cyclosporin, and an emergence of drug resistance.[20, 21] However, their clinical application value has been limited by their relatively high risk of toxicity, the emergence of drug resistance, pharmacokinetic deficiencies and/or insufficiencies in their antifungal activities. Despite recent developments [22-24], with the increase in the incidence of fungal infections and rise in azole resistance, there is still an urgent need for authentically genuine broad-spectrum and low-toxicity antifungal agents. Computer based QSAR and molecular modelling methods have been useful for the development of new molecules.[25-29] Our interest continues in azole derivatives because of higher potency and convenient for synthesis.

The set of triazole derivatives with potent inhibitory activity against lanosterol 14α-demethylase has been reported.[30] 3D-QSAR study using comparative molecular field analysis (CoMFA) and comparative molecular similarity indices analysis (CoMSIA) used to determine correlation between the structure and biological activity of these

compounds, along with that docking study were carried out to analyse interaction of compounds with binding site.[31, 32]

CoMFA is utilized to determine the correlation between steric and electrostatic fields of compounds and their biological activity.[32-35] The CoMFA is applied to a set of compounds which shows biological activity with same mechanism. At each part of the molecule and at a probe atom the steric and the electrostatic interaction energies calculated.[36]

CoMSIA method was introduced by klebe et al in 1994, which considers hydrogen bond donor, hydrogen bond acceptor and hydrophobic descriptors in addition to steric and electrostatic features.[33] To calculate similarity indices in CoMSIA, a probe atom is utilized at regular spaced grid points for the aligned compounds and Gaussian function is used for evaluation of field so, no arbitrary definition of cut-off limits. Partial Least Square method is utilized to determine cross-validated r^2 (r^2cv) and conventional r^2 values. [32, 37]

The increment in X-ray crystallographic structure deposition for the protein target leads to better structure-based drug design.[38] A molecular docking study was performed to identify the essential structural component required for interaction with CYP51.

In current work, 3D-QSAR approach is utilized to build quantitative models for prediction of the biological activity of triazole derivatives and to define the region where modification can be carried out to improve the inhibitory activity of compounds. Predictive capability of created model was determined by external validation process. Further same model was utilized to develop contour maps which provides information regarding structure activity relationship.

5.3 Material and methods

5.3.1 Datasets

A set of the 33 triazole derivatives reported as antifungal agents were taken from literature for this study.[30] Using the 'create set and random method' option in QSAR project of SYBYL-X 1.3, the compounds were divided arbitrarily into a training set of 24 compounds (70%) and a test set of 9 compounds (30%).[39] Generation of 3D-QSAR models and validation of generated models were carried out using training set and test set

respectively. The activity of compounds were assessed with MIC values i.e. IC_{80} (μgm/mL) which was converted into $pIC_{80}(-\log IC_{80})$.[40] Using Partial Least Square regression analysis the logarithmic affiliation aids to obtain symmetrically distributed data. The Structure of triazole derivatives and its biological activity data are specified in Table 5.1.

Table 5.1. Antifungal activities of triazole derivatives (1-33) used for training and test sets.

Compound no.	Compound	C.alb. inhibitory activity (μgm/mL)	pIC_{80}
1	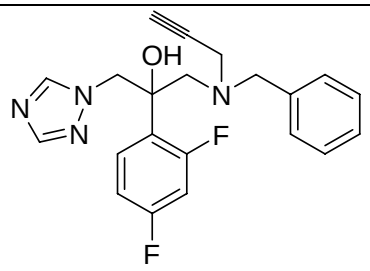	0.0039	8.408
2	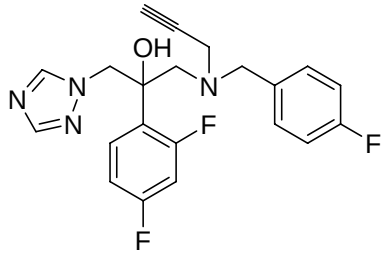	0.0156	7.806
3	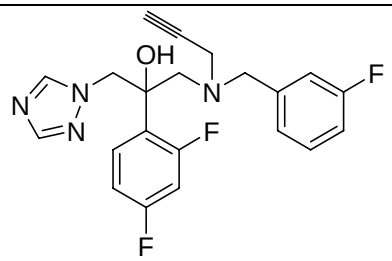	0.0039	8.408
4	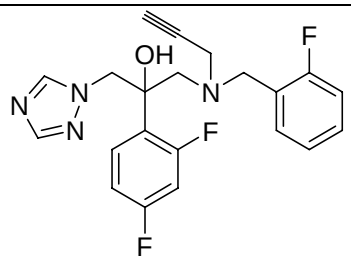	0.0156	7.806

5	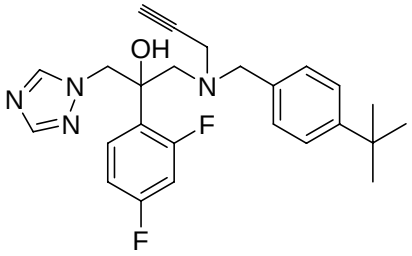	0.0156	7.806
6	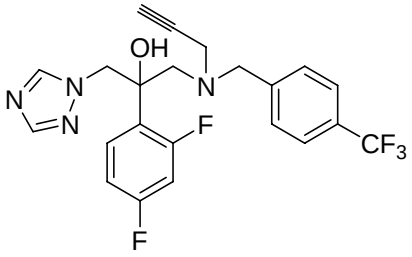	0.25	6.602
7	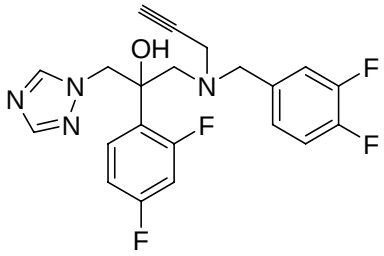	0.0039	8.408
8	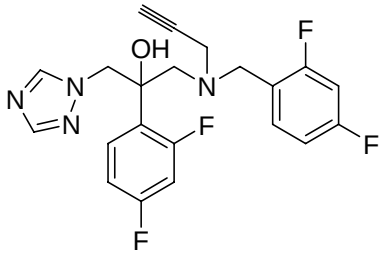	0.00097	9.013
9	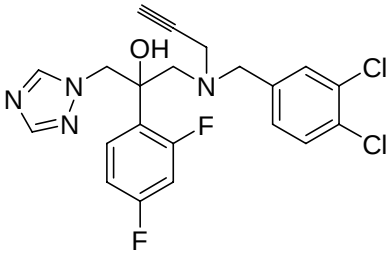	0.25	6.602
10	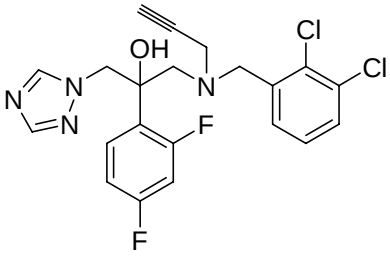	0.25	6.602

11*	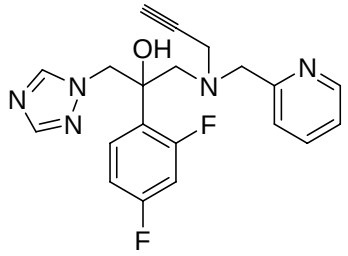	0.25	6.602
12*	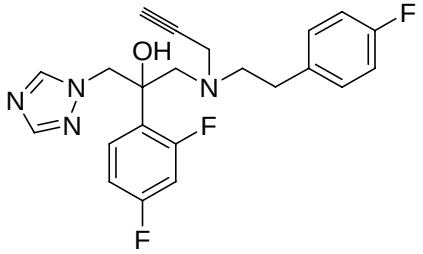	0.0625	7.204
13*	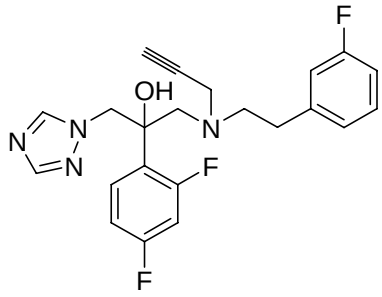	0.0625	7.204
14	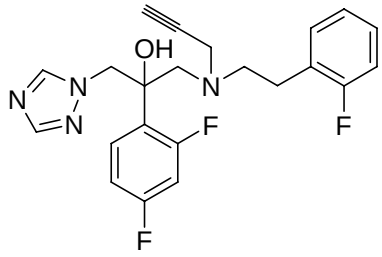	0.0625	7.204
15	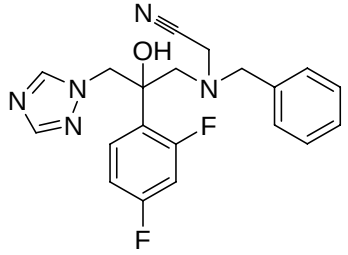	0.25	6.602
16	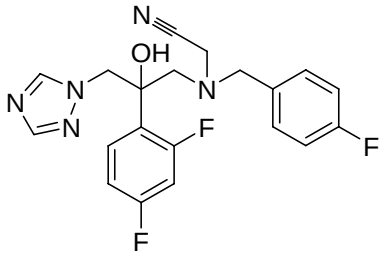	0.0625	7.204

17	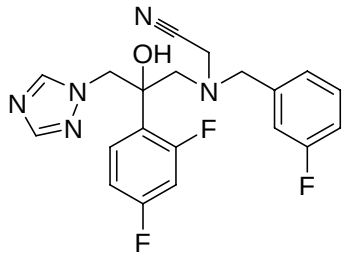	0.0156	7.806
18*	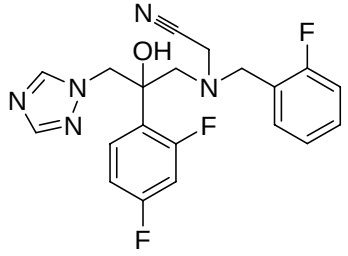	0.0625	7.204
19	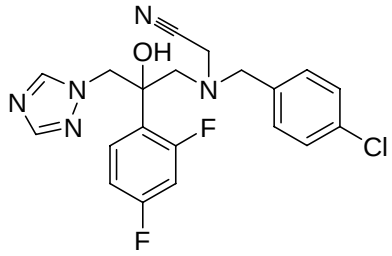	0.0156	7.806
20*	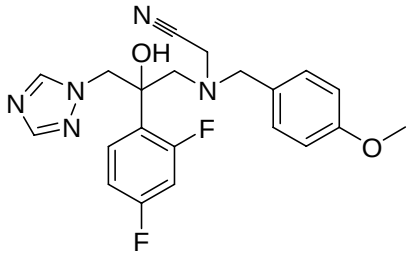	0.0625	7.204
21	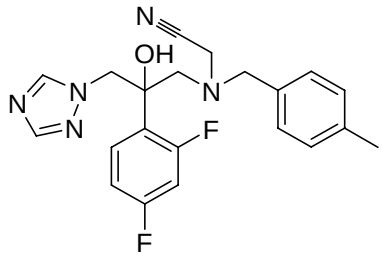	0.0625	7.204
22	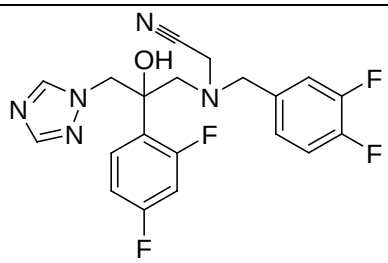	0.0625	7.204

23	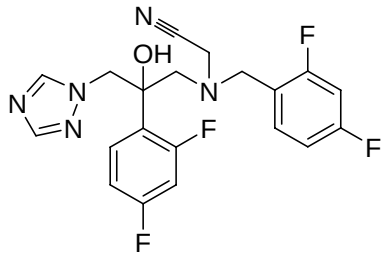	0.0625	7.204
24	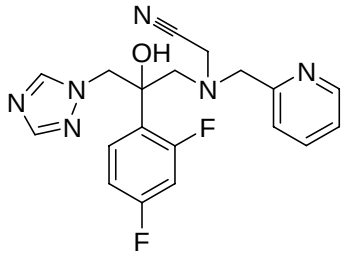	0.25	6.602
25	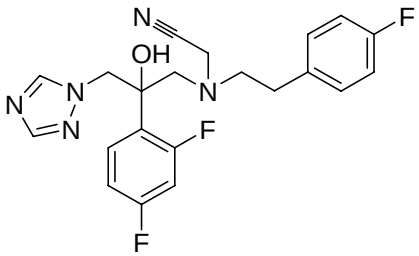	0.0156	7.806
26	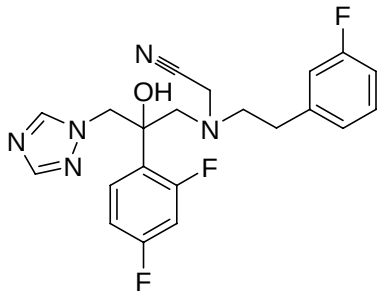	0.0625	7.204
27*	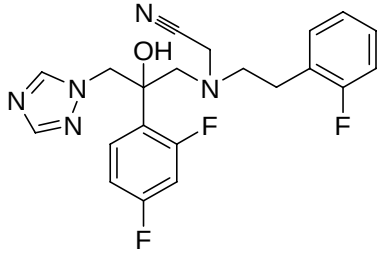	0.0625	7.204

28	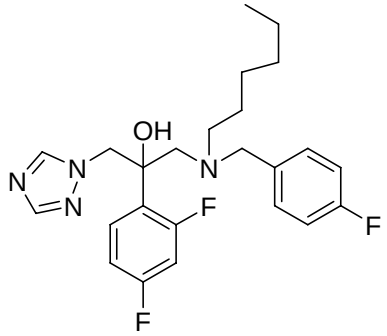	16	7.204
29*	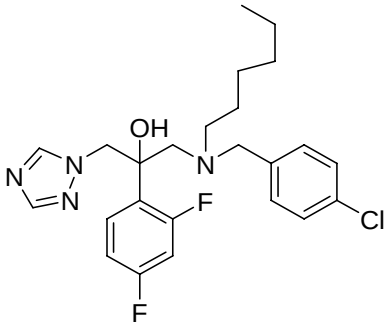	4	5.397
30*	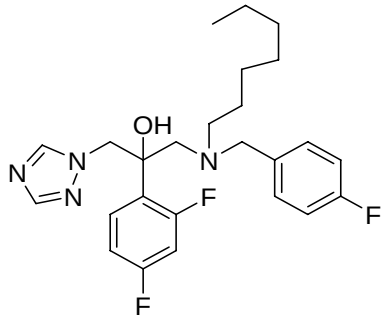	4	5.397
31*	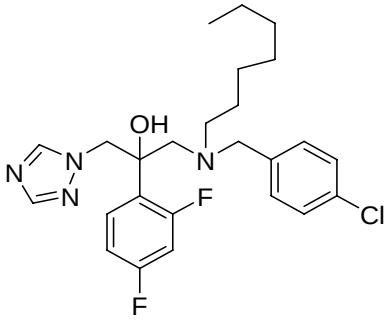	1	6.000

32	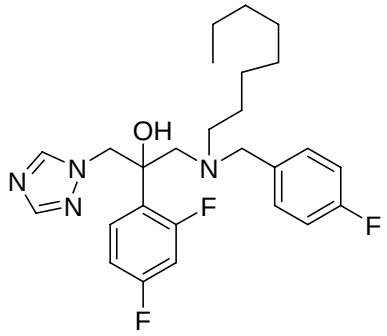	4	5.397
33	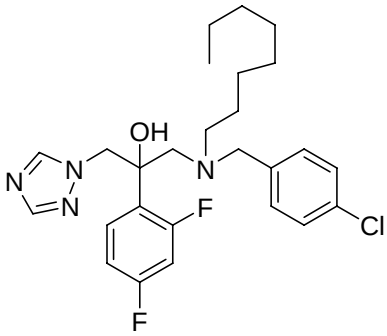	1	6.000

Note: *Test set compounds.

5.3.2 Alignment and Molecular modeling

In the study of 3D-QSAR alignment is one of the most important steps. There are numerous alignment techniques in which molecules aligned with comparable orientation and space conformation SYBYL-X 1.3 (Tripos Associates Inc, St Louis, Mo, USA) was utilized to perform all the molecular modeling study. Sketch function was used to design the 3D structure and subsequently Gasteiger-Huckel charges applied to all compounds. [41] Energy minimization was performed using the Standard tripos molecular mechanism force field.[41] Here, the distill alignment function was performed by use of SYBYL-X 1. 3. The compound 8 having the highest activity was selected as template for alignment in the data set. Therefore, all the conformers were superimposed on each other and the common core structure formed which has been represented in Figure 5.1. All the molecules are aligned which represented in Figure 5.2.

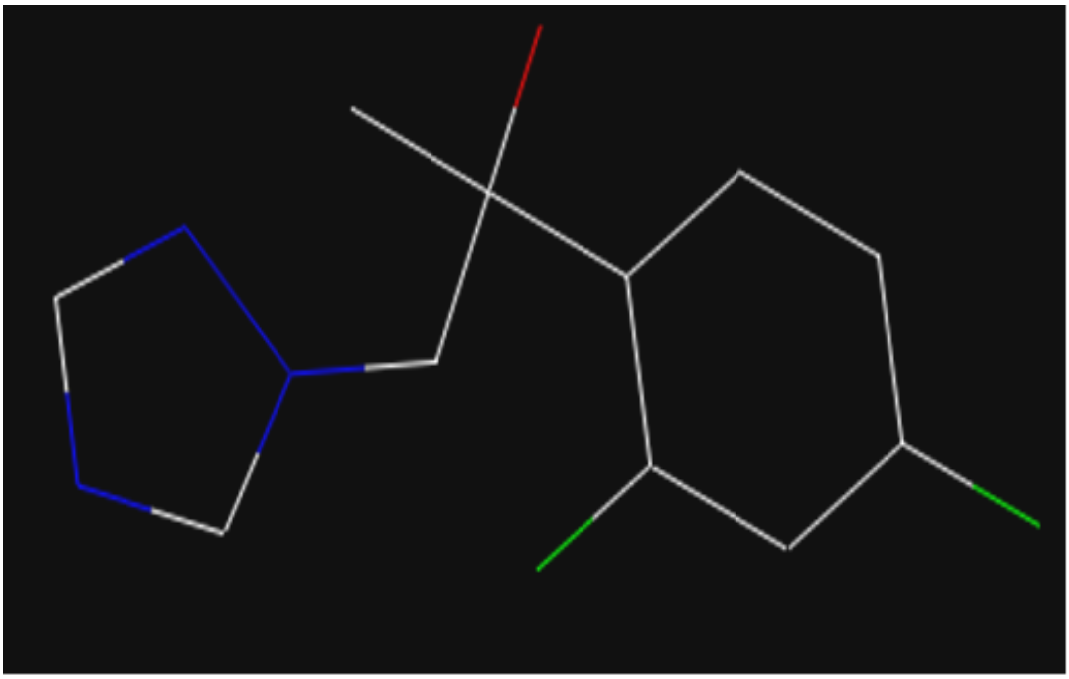

Figure 5.1. For development of CoMFA and CoMSIA models fragment utilized as a common structure for alignment of dataset.

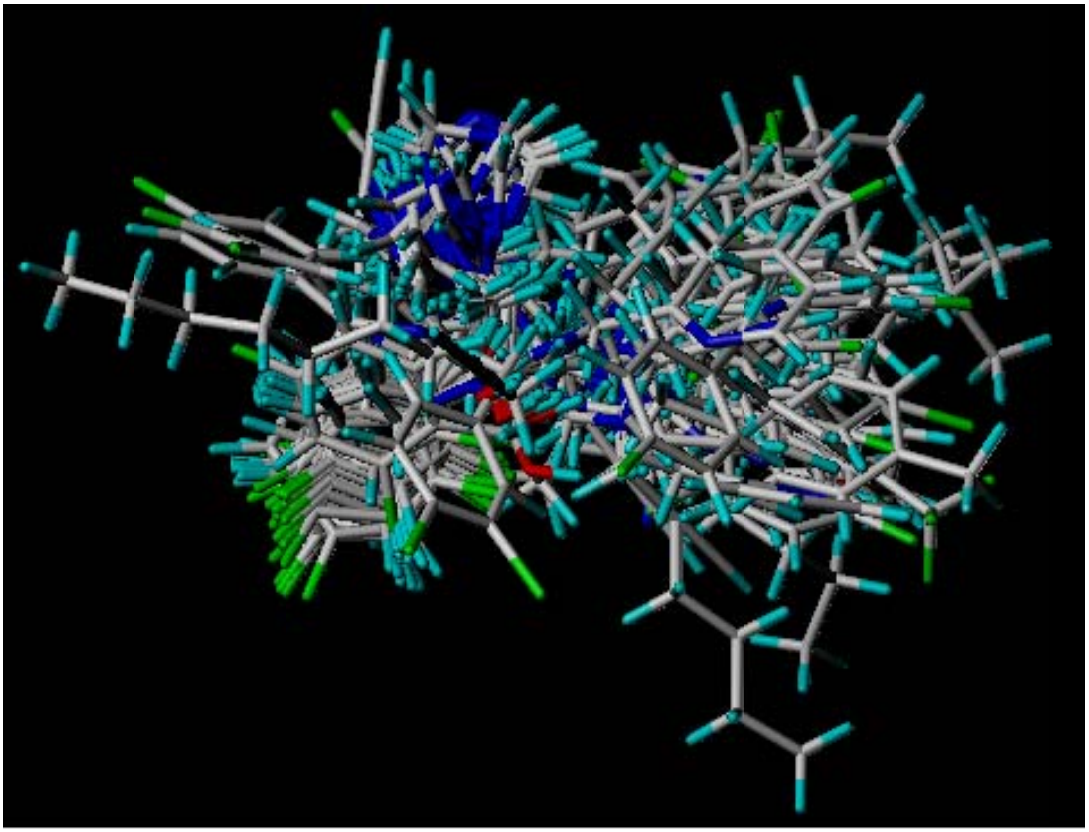

Figure 5.2. For CoMFA and CoMSIA study 1-33 aligned compounds

5.3.3 CoMFA and CoMSIA fields Generation

For each alignment, the steric and electrostatic potential fields for CoMFA were calculated at each lattice intersection of a regularly spaced grid of 2.0 Å in all X, Y and Z directions. The van der Waals potential and columbic term, which represent respectively, electrostatic and steric fields, were calculated by use of Tripos force field. A sp^3 carbon atom with van der Waals radius of 1.52 Å and +1.0 charges was served as the probe atom to calculate steric and electrostatic fields. The steric and electrostatic contributions were truncated to default ±30 kcal/mol, and the electrostatic contribution was ignored at lattice intersections with maximum steric interaction.

CoMSIA is an extension of CoMFA on the same assumption that changes in binding affinities of ligands are related to changes in molecular properties represented by the field. Besides, steric and electrostatic, hydrogen bond donor, hydrogen bond acceptor and hydrophobic descriptors are calculated in CoMSIA.[32] A Gaussian function was introduced to determine the distance between probe atom and molecular atom at all grid point similarity indices at the molecular surface can be calculated in CoMSIA. The equation for CoMSIA is as follow:

$$A_{F,K(j)}^{q} = \sum_{i} W_{probe,k}\, W_{ik} e^{-\alpha r_{iq}^{2}} \qquad (1)$$

where, A is the similarity index at grid point q, summed over all atoms i of the molecule j under investigation. W_{probe}, k is the probe atom with radius 1 Å, charge +1, hydrophobicity +1, hydrogen bond donating +1 and hydrogen bond accepting +1. W_{ik} is the actual value of the physicochemical property k of atom i. r_{iq} is the mutual distance between the probe atom at grid point q and atom i of the test molecule. α is the attenuation factor whose optimal value is normally between 0.2 and 0.4, with a default value of 0.3.[42, 43]

5.3.4 Partial least square analysis and model validation

For development of 3D-QSAR, CoMFA and CoMSIA studies were carried out using partial least square (PLS) approach which is an extension of multiple regression analysis. All the data set of definite molecules was further treated by using PLS analysis technique and development of 3D contour maps with an optimum number of components 5 equally.

PLS algorithm was used to develop the co-relation between the structural property and biological activity. By use of PLS analysis, leave one out (LOO) and cross-validation analysis was performed. In cross-validation method one molecule is subtracted from the data set and its activity is predicted referencing the model obtain from rest of the data set. The cross-validation coefficient is represented as q^2. The models were accepted if model provides value of $q^2 > 0.5$ and $r^2 > 0.641$.[44] It is generally estimated as:

$$q^2 = 1 - \frac{\sum \left(Y_{predicted} - Y_{observed}\right)}{\sum \left(Y_{observed-} Y_{mean}\right)} \quad (2)$$

While, the validation of conventional correlation co-efficient r^2, standard error of estimate (SEE) and F values were carried out in non-cross validation method. At the end bootstrap analysis was performed to check the robustness of the generated model, It is a method which carried out numerous times (for good statistical information 100 times required) in which n random selections are carried out from the original set of n object,. During every run, certain molecules can be omitted from the Partial Least Square analysis, while remaining molecule must be involved many times. Bootstrap r^2 (r^2_{bs}) represented mean correlation coefficient. For CoMFA and CoMSIA analysis cross-validation (r^2_{cv}) was carried out by two groups ('leave half out' method).

5.3.5 Predictive correlation coefficient (r^2_{pred})

The test set of nine compounds was used to determine the predictive power of generated 3D-QSAR model. Template was used to align the compounds and their pIC_{80} values were predicted. Based on the test set compound the predictive correlation coefficient (r^2_{pred}) was determined by the following equation:

$$r^2_{pred} = \frac{(SD - PRESS)}{SD} \quad (3)$$

where, SD is the totality of squared deviation between biological activity of the test set compounds and mean activities of the training set compounds, and PRESS is the totality of squared deviations between experimental and predicted activity values for each compound in the test set.

5.3.6 Docking

In the current study, Glide 5.8 (Schrodinger, LLC, New York) accessed on Windows 7 was utilized for preparation of protein and docking study.[45] The deposited crystal structure of Lanosterol 14α-demethylase (CYP51) complex with inhibitor was retrieved from Protein Data Bank (PDB: 1AE1). After introducing, the protein was treated under several structure requirements such as bond assignment and bond order, hydrogen addition, chains filling, bond adjustment and addition of charges to metal and correction of mislabeled components. To augment the absent residues in the side chain Maestro was utilized. In structure of protein Water molecules were deleted and subsequently, hydrogen added. In the structure, steric clashes present so protein structure minimization was performed by utilization of Impact Refinement module, incorporating the OPLS 2005 (Optimized Potential for Liquid Simulation) force field. While, minimization was finished when RMSD (Root Mean Square Deviation) reaches to a cut-off of 0.30 Å.

Receptor grid was generated by receptor grid generation panel. To recognize the active site, the ligand was selected to define the position and size of active site. The interaction site is represented by rectangular box enclosing the translations of the mass centre of the ligand. Orientations and conformations of the ligand in the binding site were done using Glide (Grid-based Ligand Docking with Energetics).[46, 47]

Maestro 9.3 and LigPrep 2.5 were accessed for building ligand and preparation respectively.[48, 49] Before docking study, conversion of 2D structure into 3D, generation of stereoisomer, neutralization of charged structures and addition of hydrogen were carried out with help of ConfGen by introducing OPLS-2005 force field. Monte-Carlo Multiple Minimum (MCMM) / Low Mode (LMOD) with per structure maximum 1000 conformers and 10000 minimization steps were utilized for exploration of Conformational space.[50, 51]

5.4. Results and discussion

5.4.1 CoMFA studies

The training set and test set was utilized to developed CoMFA model. For model, Partial Least Square method was carried out with Leave One leave out which demonstrated the value of q^2 0.611 through optimum 5 components. Column filtering 2.0 and same five components was utilized for Non cross-validated (r^2_{ncv}) PLS analysis, which gives r^2_{ncv} =

0.982, significance value (*F*) = 296.835, standard error of estimation (SEE) = 0.140 and predictive power r^2_{pred} of 0.871. A contribution of Steric and electrostatic fields were found to be 1.246 and 1.518, respectively. Obtained results obtained throw CoMFA analysis are represented in Table 5.2. The Cross-validation and bootstrapping result strongly support reliability of The CoMFA model. The experimental and predicted pIC_{80} values for the training set and test set are shown in Table 5.4 and 5.5 respectively, and the experimental and predicted activities correlation in the form of scatter graphs are presented in Figures 5.3 and 5.4 respectively.

Table 5.2 Statistical parameter by using PLS analysis for CoMFA.

PLS analysis parameter	*CoMFA*
r^2_{loo} (q^2)	0.611
ONC	5
SEE	0.14
r^2_{ncv}	0.982
F value	296.835
Steric field contribution	1.246
Electrostatic field contribution	1.518
r^2_{bs}	0.991
SEE_{bs}	0.005
r^2_{cv}	0.520
Test set r^2_{pred}	0.871

Table 5.3 Statistical parameter by using PLS analysis for CoMSIA.

PLS analysis parameter	*CoMSIA*
r^2l_{oo} (q^2)	0.792
ONC	5
SEE	0.228
r^2_{ncv}	0.953
F value	109.480
Steric field contribution	0.164

Electrostatic field contribution	0.450
Hydrophobic field contribution	0.385
Hydrogen bond donor	0.700
Hydrogen bond acceptor	0.390
r^2_{bs}	0.972
SEE_{bs}	0.013
r^2cv	0.745
Test set r^2_{pred}	0.752

5.4.2 CoMSIA studies

Same training set and test set was utilized for CoMSIA model development because, significant results found with CoMFA. Steric, electrostatic, hydrophobic, hydrogen bond acceptor and hydrogen bond donor fields were used for generation of CoMSIA model. The cross-validation (q^2) value for CoMSIA model was obtained 0.792 by five optimum numbers of components (ONC). Column filtering 2.0 and Similar five components was utilized for Non cross-validated (r^2_{ncv}) PLS analysis, resulting in r^2_{ncv} = 0.953 and SEE = 0.228. The steric contribution = 0.164, electrostatic contribution = 0.45, hydrophobic contribution = 0.385, hydrogen bond donor = 0.7, hydrogen bond acceptor = 0.39. Predictive power of CoMSIA r^2_{pred} was found to be 0.752. Leave half out cross-validation method and boot strapping analysis was performed to determine the quality of developed model. For the CoMSIA r^2_{cv} was found to be 0.745. To analyze the internal reliability within the dataset the mean r^2 value of boot strapping analysis (boot strapped r^2_{bs}) and SEE_{bs} were performed which was found to be 0.972 and 0.013 respectively. Statistical parameter obtained throws CoMSIA model is represented in Table.5.3 According to the CoMSIA model experimental and predicted pIC_{80} values for training set and test set are represented in Table. 5.4 and 5.5 respectively while, the relationships between experimental and predicted inhibitory activities are represented in the form of scatter graphs in Figures 5.3 and 5.4 respectively.

Table 5.4 Experimental, predicted pIC_{80} and residual values of training set compounds by CoMFA and CoMSIA analysis.

		CoMFA		*CoMSIA*	
Compound no.	*Experimental value*	*Predicted*	*Residual*	*Predicted*	*Residual*
1	8.409	8.293	0.115	8.319	0.089
2	7.806	7.804	0.002	7.578	0.228
3	8.408	8.495	-0.086	8.455	-0.046
4	7.806	7.493	0.313	7.884	-0.077
5	7.806	7.789	0.017	7.684	0.122
6	6.602	6.649	-0.041	6.873	-0.271
7	8.408	8.608	-0.199	8.866	-0.457
8	9.013	9.020	-0.006	8.527	0.486
9	6.602	6.630	-0.028	6.526	0.076
10	6.602	6.691	-0.089	6.459	0.143
14	7.204	7.212	-0.007	7.447	-0.242
15	6.602	6.916	-0.314	7.021	-0.419
16	7.204	7.406	-0.201	7.213	-0.008
17	7.806	7.762	0.044	7.829	-0.022
19	7.806	7.750	0.056	7.736	0.070
21	7.204	7.233	-0.028	7.008	0.198
22	7.204	7.240	-0.035	7.185	0.019
23	7.204	7.144	0.060	7.353	-0.148
24	6.602	6.622	-0.020	6.708	-0.106
25	7.806	7.553	0.253	7.515	0.291
26	7.204	7.082	0.122	7.099	0.105
28	4.795	4.741	0.054	5.098	-0.302
32	5.397	5.518	-0.120	5.400	-0.002
33	6.000	5.895	0.105	5.690	0.310

Table 5.5 Experimental, predicted pIC_{80} values and residual values of test set compound by CoMFA and CoMSIA analysis.

		CoMFA		*CoMSIA*	
Compound no.	*Experimental value*	*Predicted*	*Residual*	*Predicted*	*Residual*
11	6.602	6.593	0.009	6.349	0.253
12	7.204	7.206	-0.001	7.038	0.166
13	7.204	7.357	-0.152	7.337	-0.132
18	7.204	7.115	0.089	7.355	-0.150
20	7.204	7.051	0.153	7.248	-0.043
27	7.204	7.211	-0.006	7.287	-0.082
29	5.397	5.258	0.139	5.307	0.090
30	5.397	5.665	-0.267	5.556	-0.108
31	6.000	6.025	-0.025	5.974	0.026

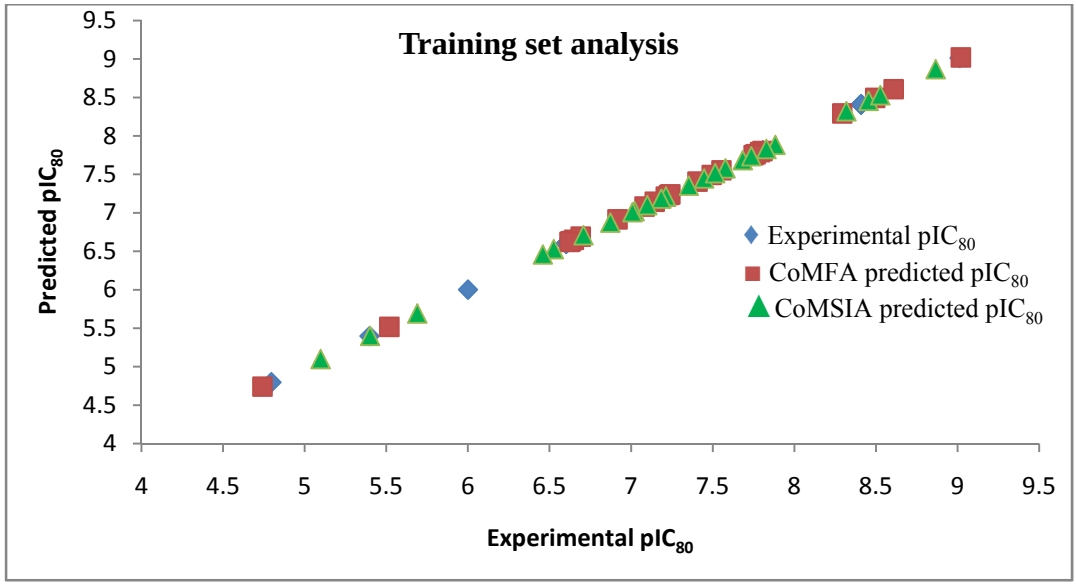

Figure 5.3 Graph of actual and predicted pIC_{80}value for training set by CoMFA and CoMSIA analysis.

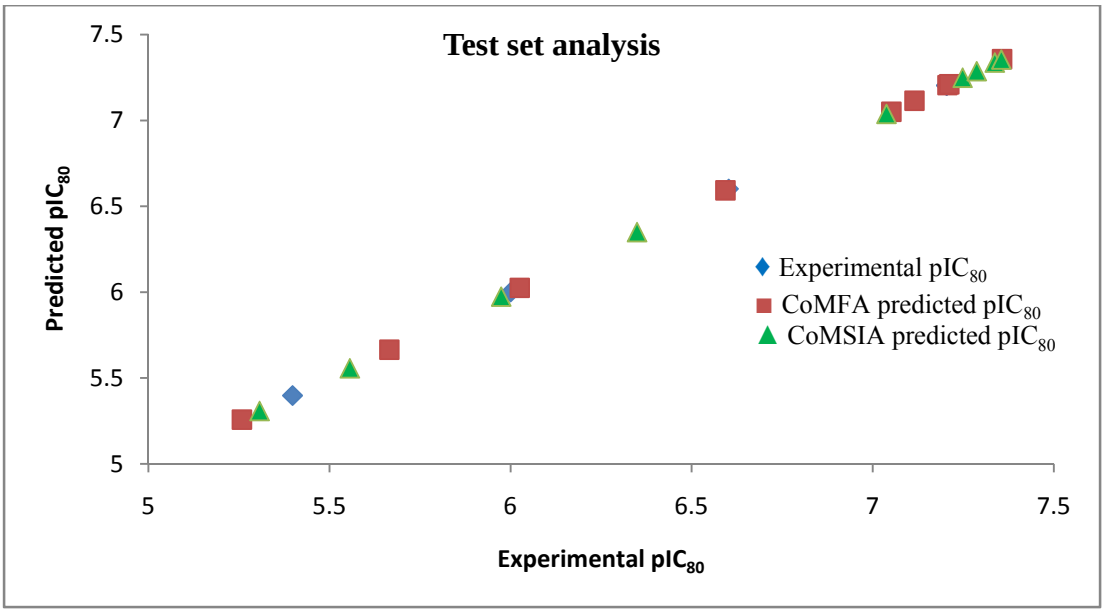

Figure 5.4 Graph of actual and predicted pIC_{80} values for test set by CoMFA and CoMSIA analysis.

5.4.3 3D-QSAR visualization

5.4.3.1 CoMFA

The significant feature of CoMFA model is the outcomes obtained by 3D coefficient contour maps which are calculated as the variation in the molecular fields multiplied by the 3D-QSAR coefficient by using Model stDev*Coeff. CoMFA contour maps were generated to identify the important regions in 3D space surrounding the molecules, so that modification can be carried out in those areas to increase the inhibitory activity, which may be utilized to improve CYP51 inhibitory activity.

The most active compound 8 and least active compound 28 were used to generate contour maps by managing style of contour to transparent for better analysis of contour surrounding compound 8 which represented in Figures 5.6 (a, b) and for compound 28 represented in Figure 5.6 (c, d) includes steric and electrostatic region respectively. The steric region signs two colours in contour maps i.e. green and yellow. In which green color indicates the favourable part, keeping the bulkier group which leads to an increase in the biological activity whereas; yellow color indicates a decrease in the biological activity due to the bulkier region. Further, the electrostatic contour map shows red and blue color. The red color and blue color indicates the favourable and unfavourable region

respectively. Here, red color region indicates that biological activity enhanced by negative charge while, blue color region indicates positive charge leads to increase in biological activity.

5.4.3.2 CoMSIA

CoMSIA contour maps were generated similarly as Contour maps generated by CoMFA. For the CoMSIA total 5 contour maps were generated, for steric, electrostatic, hydrophobic, donor and acceptor fields. The steric and electrostatic region has the same description like CoMFA. Whereas; the hydrophobic has yellow and white color codes in which yellow color indicate hydrophobic group favorable; while white color indicates hydrophobic group unfavorable. The donor has cyan and purple color; cyan color indicates donor group favorable; while purple indicates acceptor group favorable. They show which part/substitute help to find out the favorable and unfavorable region.

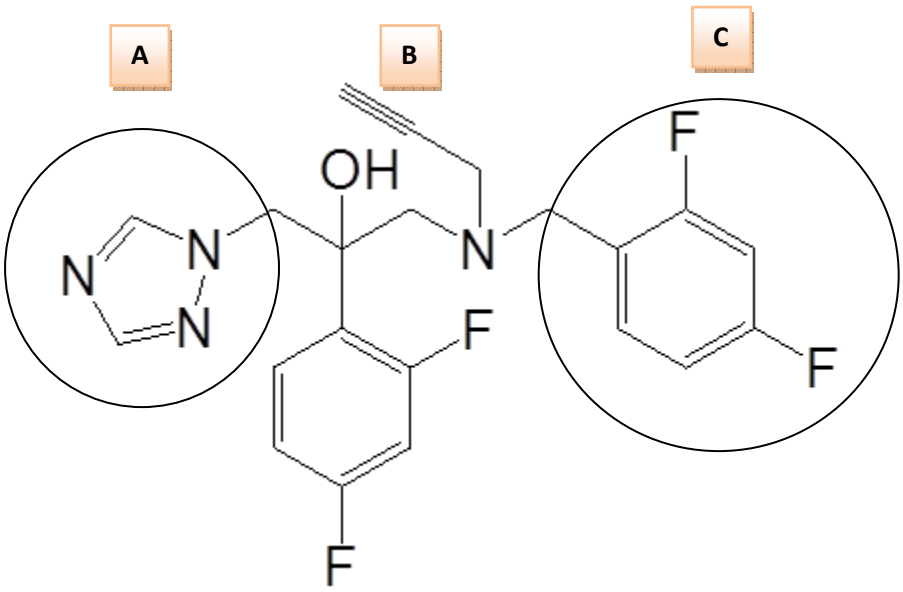

Figure 5.5 Most potent compound 8 distributed into (A), (B) and (C) regions.

5.4.3.3 Analysis of CoMFA and CoMSIA contour map

5.4.3.3.1 CoMFA

Figure 5.6(a, c) depicts the CoMFA steric contour plot. Whereas, Figure 5.5 represents most active compound 8 is divided into three major regions (**A**, **B** and **C**). A large green contour found surrounding area **B** suggests that the addition of a more bulky group in this area is favorable for activity, which elucidates the requirement of the steric interaction of the ligand with the receptor. Similarly green contour at N atom substituent indicates that bulky group is favored at this position, but increase in the length of the substituent on N more than 3 carbon atoms leads to decrease in the biological activity. Experimental inhibitory activity values for compounds 28-33 strongly supports this, in which large bulky group present as compare to other compounds 1-27.

A yellow contour at **C** region in substituted phenyl ring at C-5 and C-6 position indicates the bulky group is not favored at this region leads to decrease in activity. As depicted in Figure 5.6c for compound 28, in which the bulky substituent at N atom which shows yellow contour therefore, remarkable decrease in the biological activity.

Figure 5.6(b, d) displays the electrostatic contour map using CoMFA. The electrostatic field characterized by red and blue contour map. The most active Compound 8 was selected which represented in figure 5.6b, a blue contour surrounding area **A** at triazole ring specifies that need for positively charged substituent to produce potent antifungal activity. Similar blue contour near **B** region at N atom substituent and near **C** region in substituted phenyl ring at C-3 and C-4 position indicate the introduction of positively charged substituent increase the activity. While, red contour near region **B**, in diflurophenyl ring at C-1 and C-5 Position, indicating the introduction of negatively charged group leads to increase in the activity.

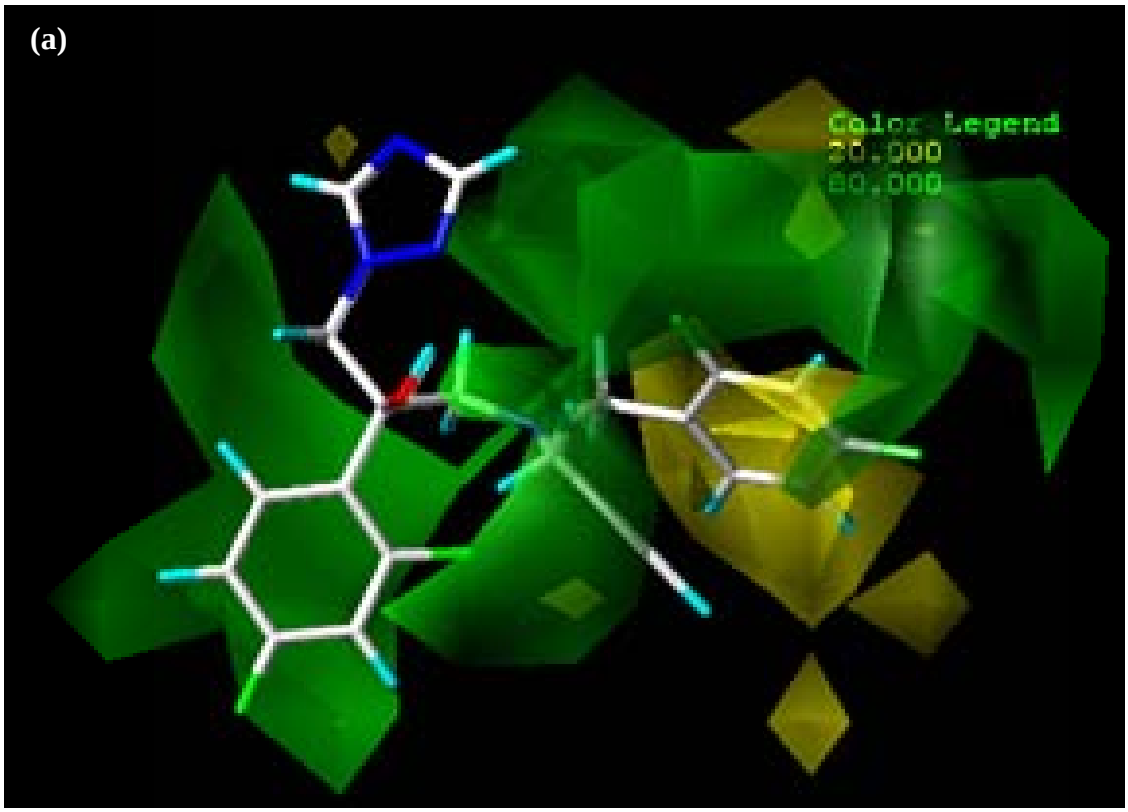
(a)
Color Legend
20.000
80.000

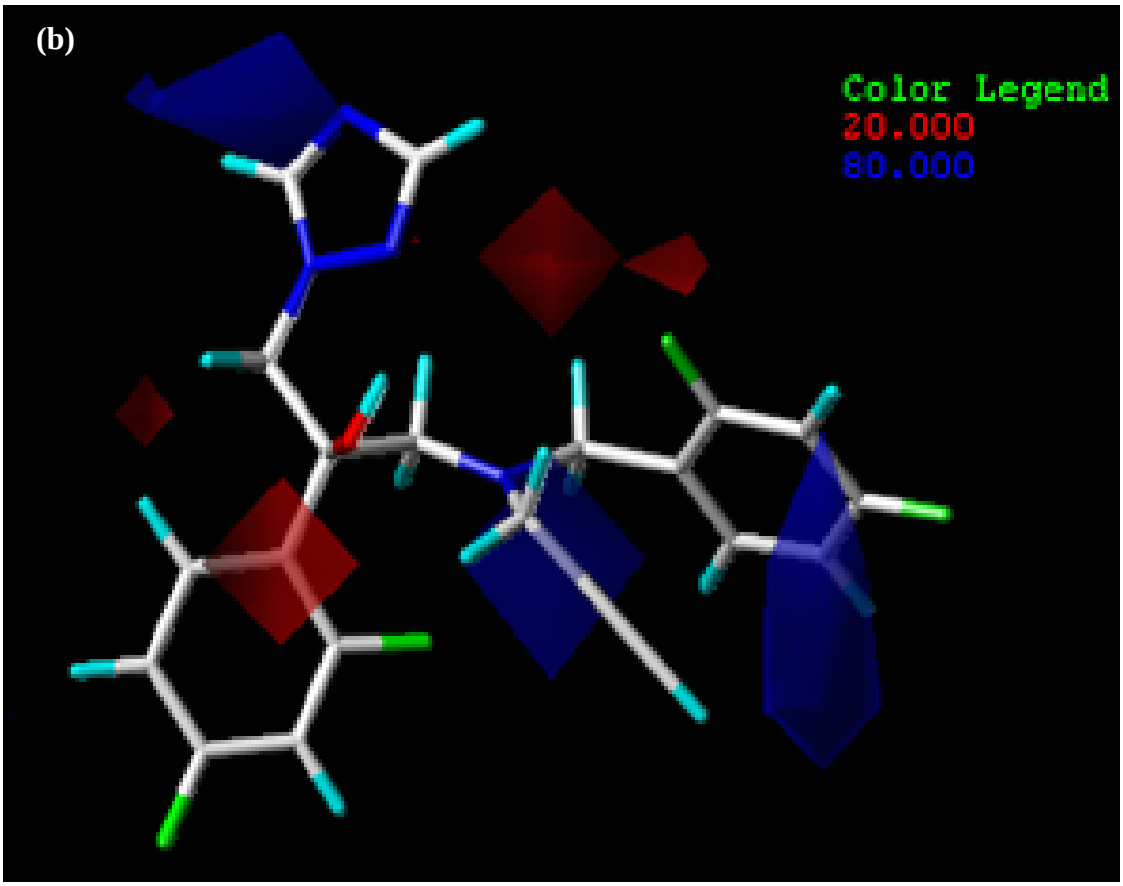
(b)
Color Legend
20.000
80.000

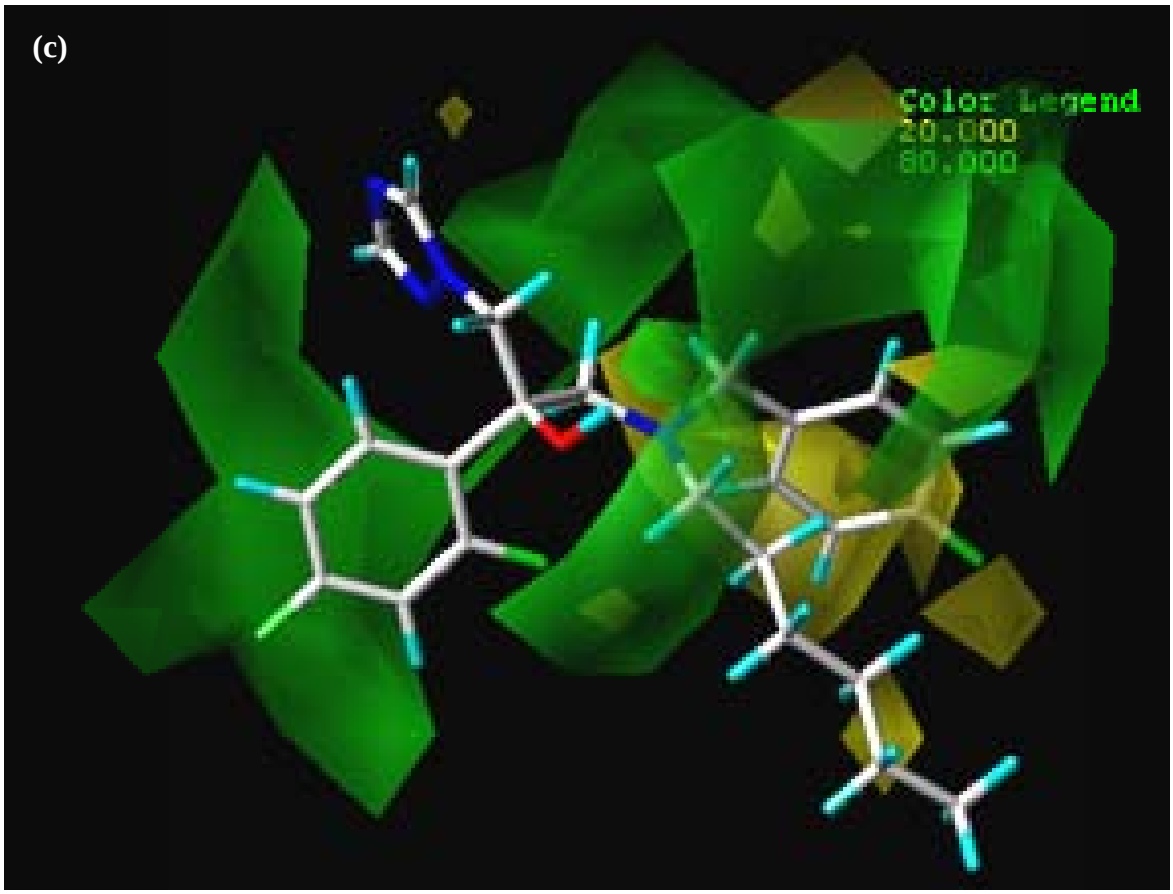
(c)
Color Legend
20.000
80.000

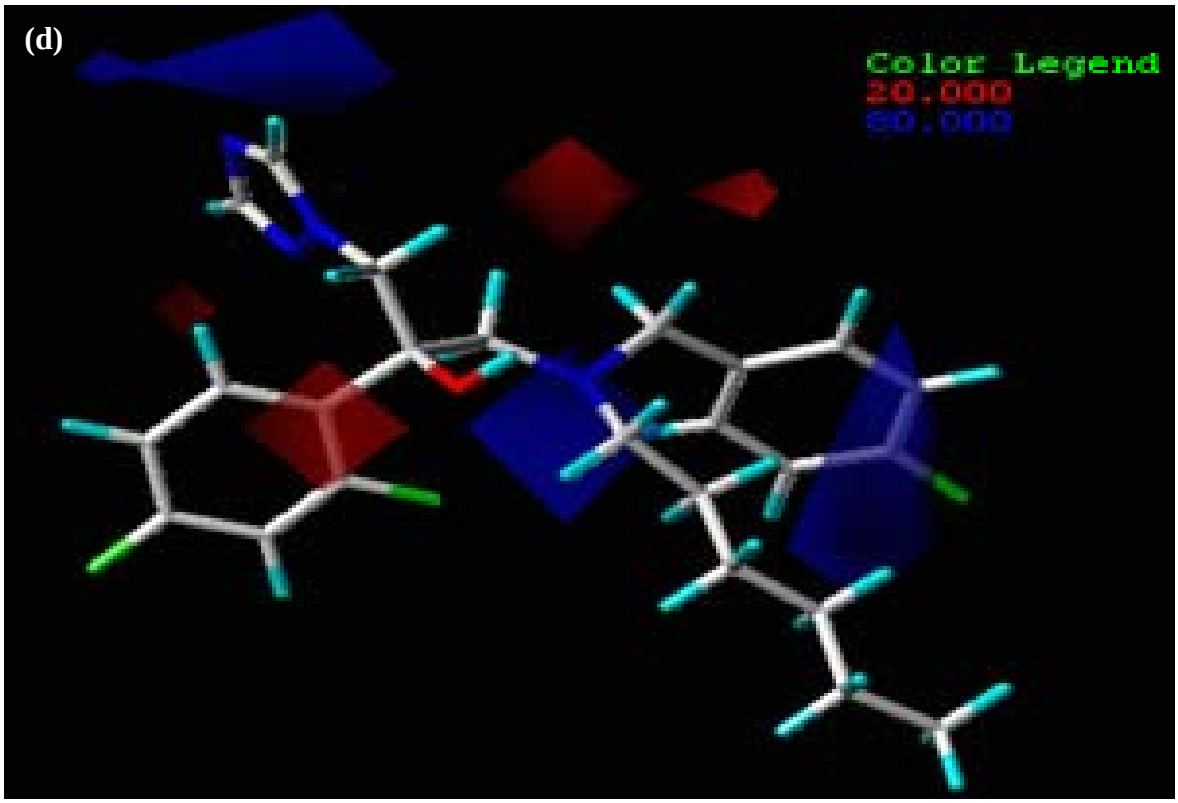
(d)
Color Legend
20.000
80.000

Figure 5.6. Steric contour maps (a,c) and electrostatic contour maps (b, d) generated by comparative molecular field analysis (CoMFA) for the most active compound 8(a, b) and the less active compound 28(c,d), respectively.

5.4.3.3.2 CoMSIA

Steric field and electrostatic fieldfor CoMSIA method stand similar as found in the CoMFA. In addition to that further details are given. The yellow contour seen near the terminal position in N atom substituent at **B** region represents that the large bulky group is not favorable in this part for better activity. The large bulky group present in this part in the least active compound of the data set, compound 28, as represented in Figure 5.7a. Further, it is supported by experimental inhibitory activity data for compunds 28 to 33,which have the large bulky group at this position than compounds 1-27. In Figure 5.7b, the red contour at triazole linking at **A** region indicating that replacement of hydrogen atoms with negatively charged atom leads to increase in the activity. Further near **C**-region in phenyl ring at the C-2 position more negatively charged substituent leads to increase in the activity.

While, in CoMSIA hydrophobic contour map the yellow region suggest that hydrophobic substituent in this part increases biological activity and white contour map suggests that hydrophilic group will enhance activity. From Figure 5.7c, the yellow contours for compound 8 seen in **B** and **C** region indicate hydrophobic and bulky functional groups are favourable in this region. But it surrounded by small white contour indicating very large bulky group leads to decrease in the activity. While in **B** region at N atom substituent white contour map indicate hydrophilic substituent are favoured in this area. It is suggested from the experimental activity data for compounds 28-33 in which large bulky group present at this region while in compounds 1-28 have a small bulky group so significant difference in inhibitory activity.

As display in Figure 5.7d, the minor cyan contour is seen at linker between the N atom and substituted phenyl ring in **C** region indicating that replacement of H atom with the hydrogen bond donor leads to increase in inhibitory activity. Similarly, in **B** region, cyan

contour at the C-2 position in difluro-substituted phenyl ring indicate hydrogen bond donor will increase the inhibitory activity of the compound.

In Figure 5.7e, a magenta contour was seen near the **A** region in the triazole ring which indicate substituents with hydrogen bond acceptor property will lead to increase in biological activity. Similarly, at linker between N Atom and the carbon atom in **B** region also show magenta contour which shows that hydrogen bond acceptor substituent at this region leads to increase in activity while, red contour at hydroxyl group near **B** region indicating that replacement of hydroxyl group with hydrogen bond acceptor leads to increase in the inhibitory activity.

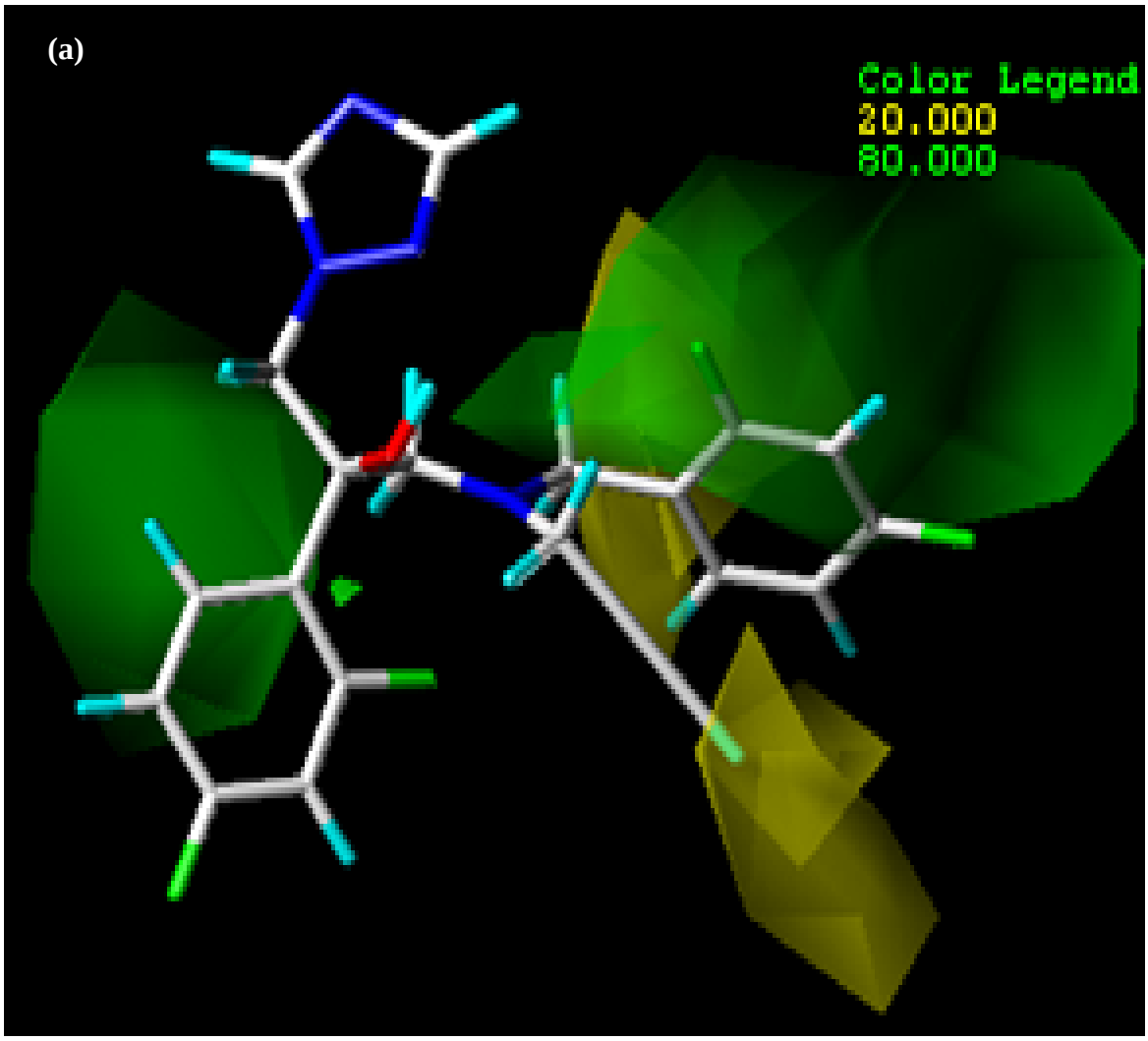

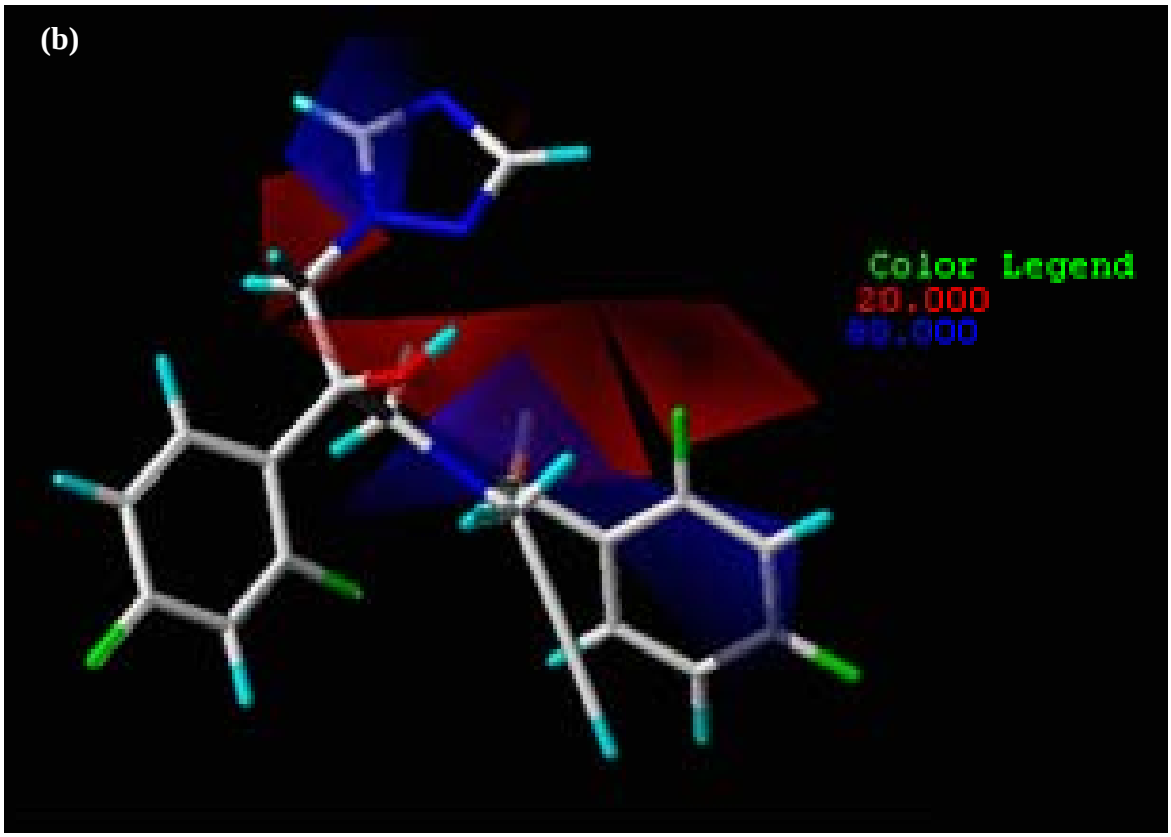
(b)
Color Legend
20.000
80.000

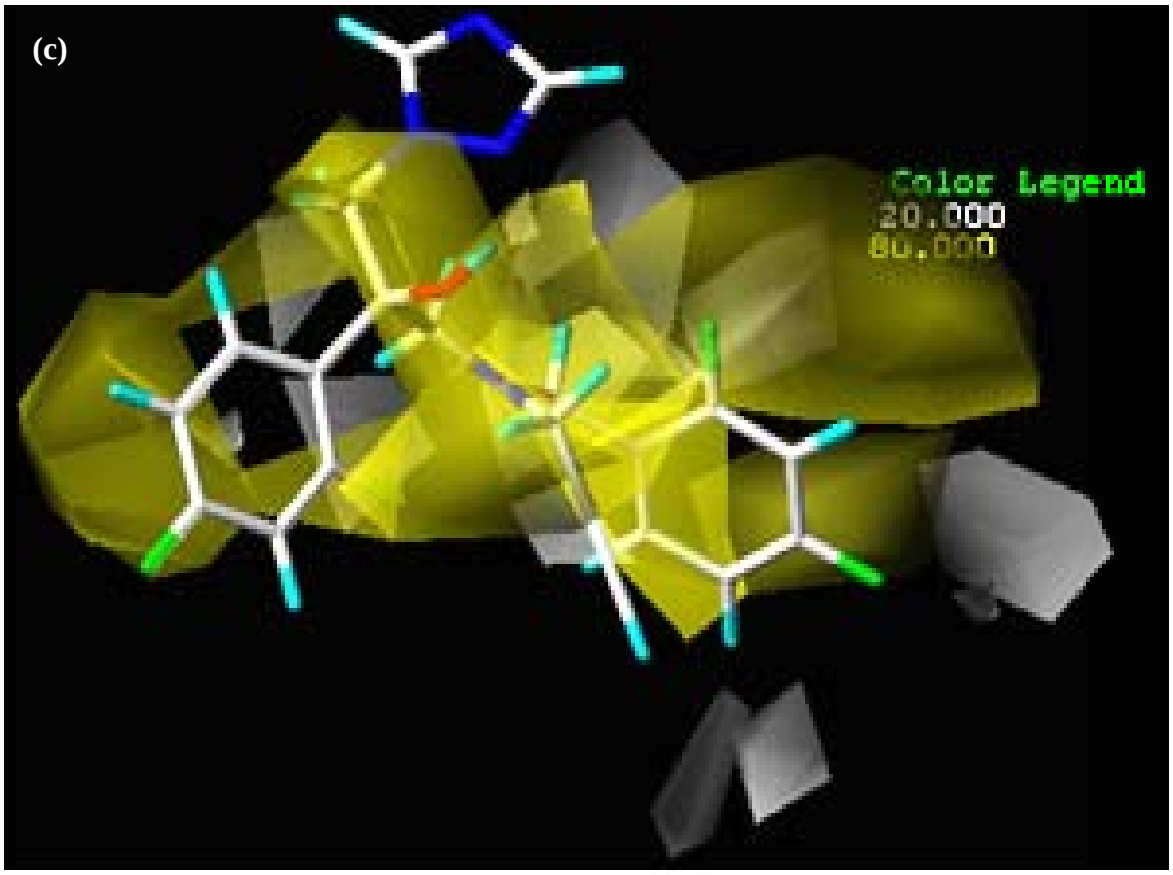
(c)
Color Legend
20.000
80.000

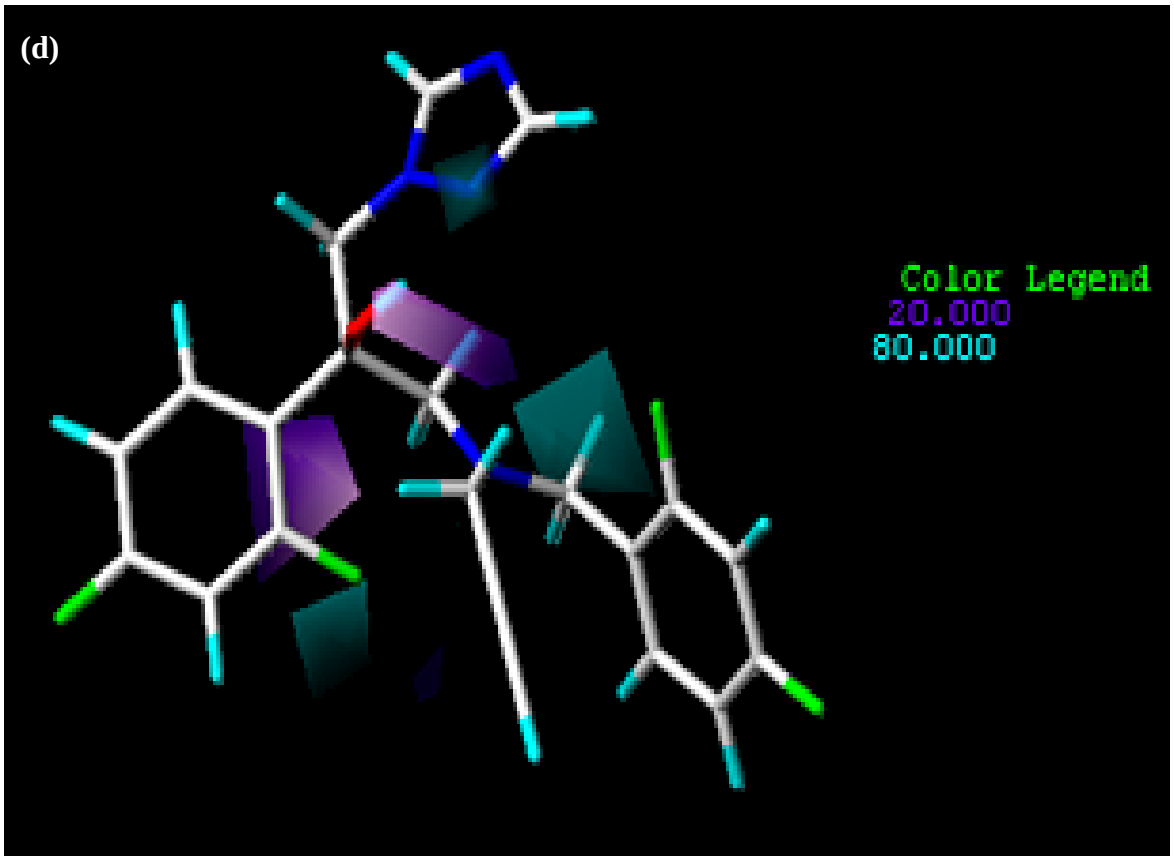
(d)
Color Legend
20.000
80.000

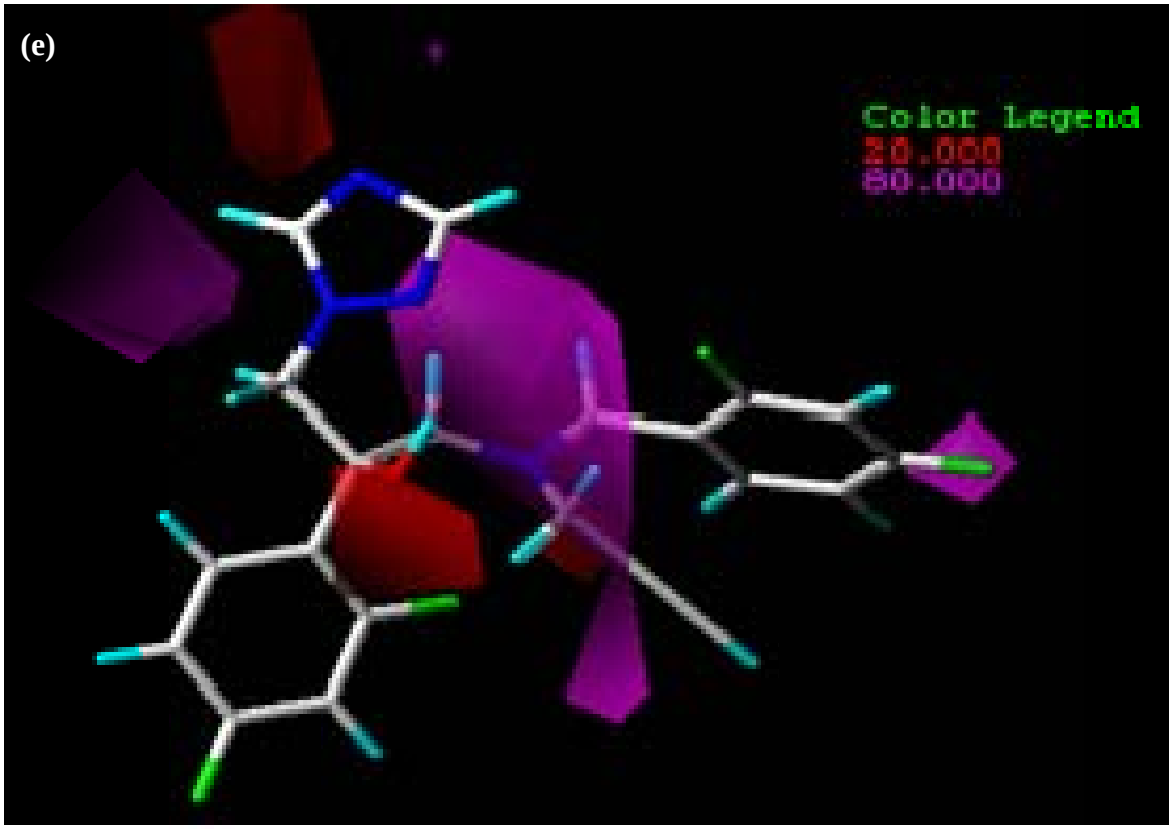
(e)
Color Legend
20.000
80.000

Figure 5. 7. Comparative molecular similarity indices analysis (CoMSIA) for most active compound 8(a) Steric map (green, bulky group desirable; yellow, bulky group not desirable), (b) electrostatic map contour map (blue, electropositive group desirable; red, electronegative group desirable), (c) hydrophobic map (yellow, hydrophobic group desirable; white, hydrophilic group desirable), (d) donor map (cyan, donor group desirable; purple, donor group undesirable and (e) acceptor map (magenta, acceptor group desirable; red, acceptor group undesirable).

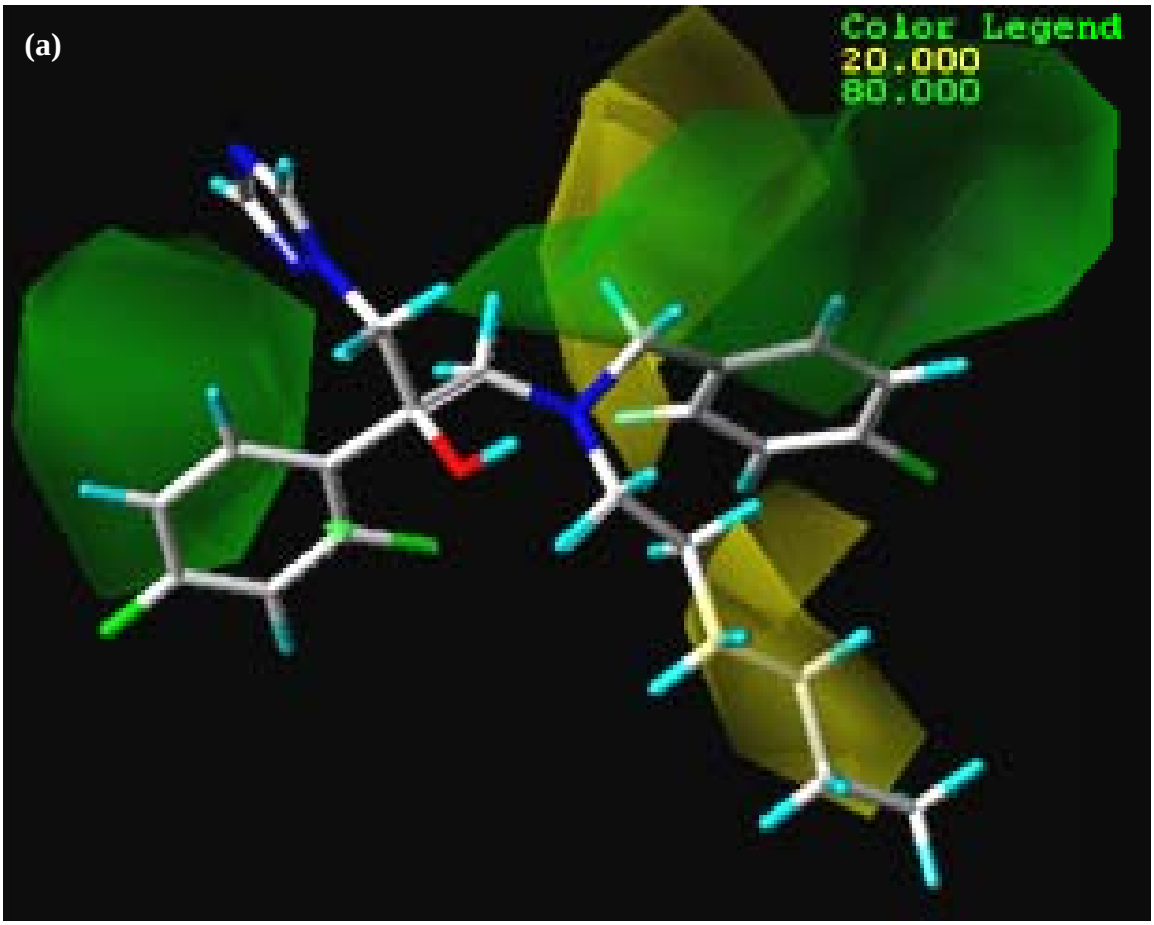

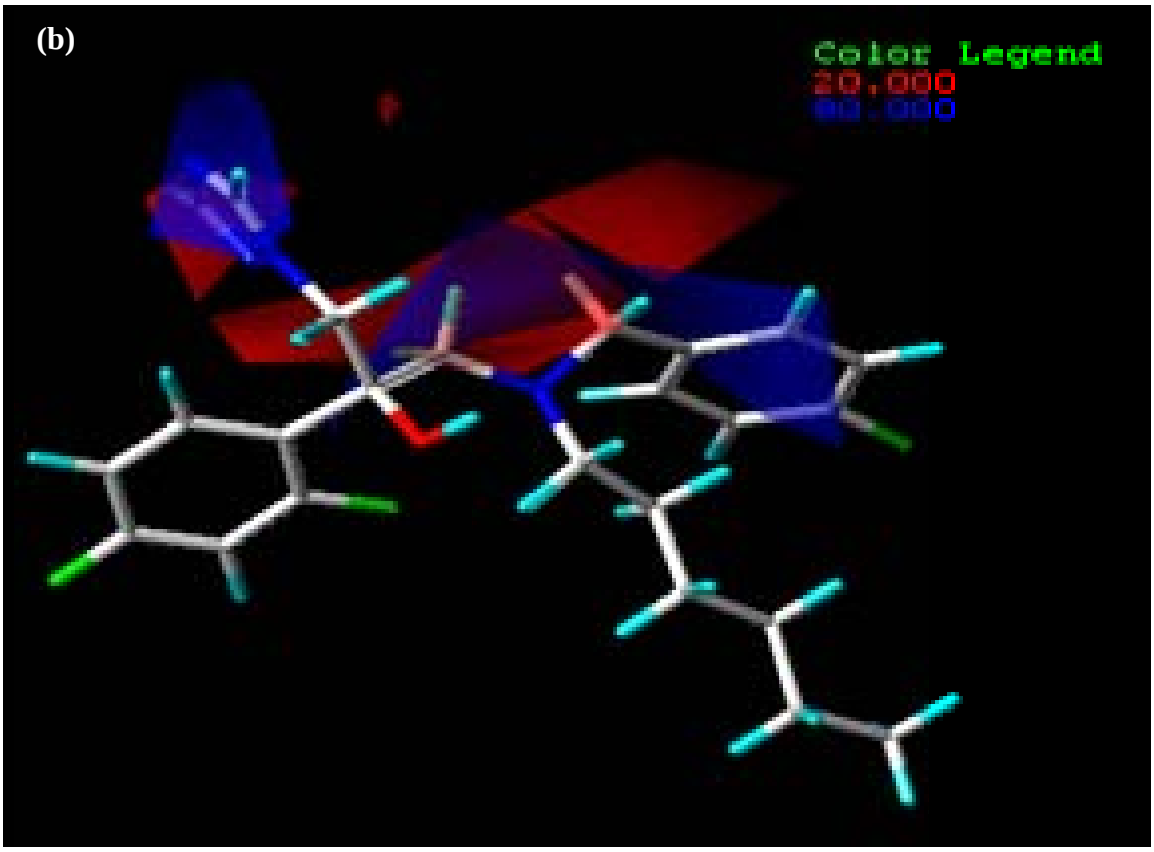
(b)
Color Legend
20.000

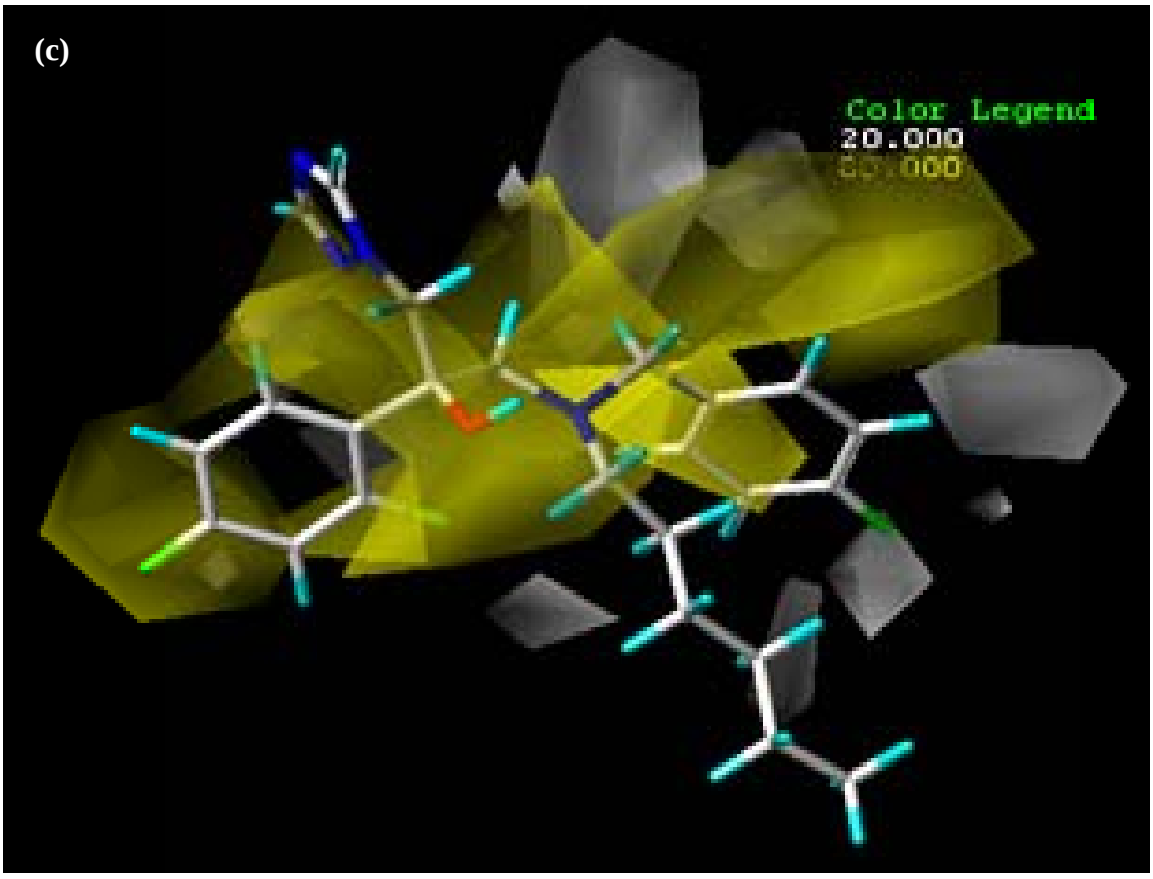
(c)
Color Legend
20.000

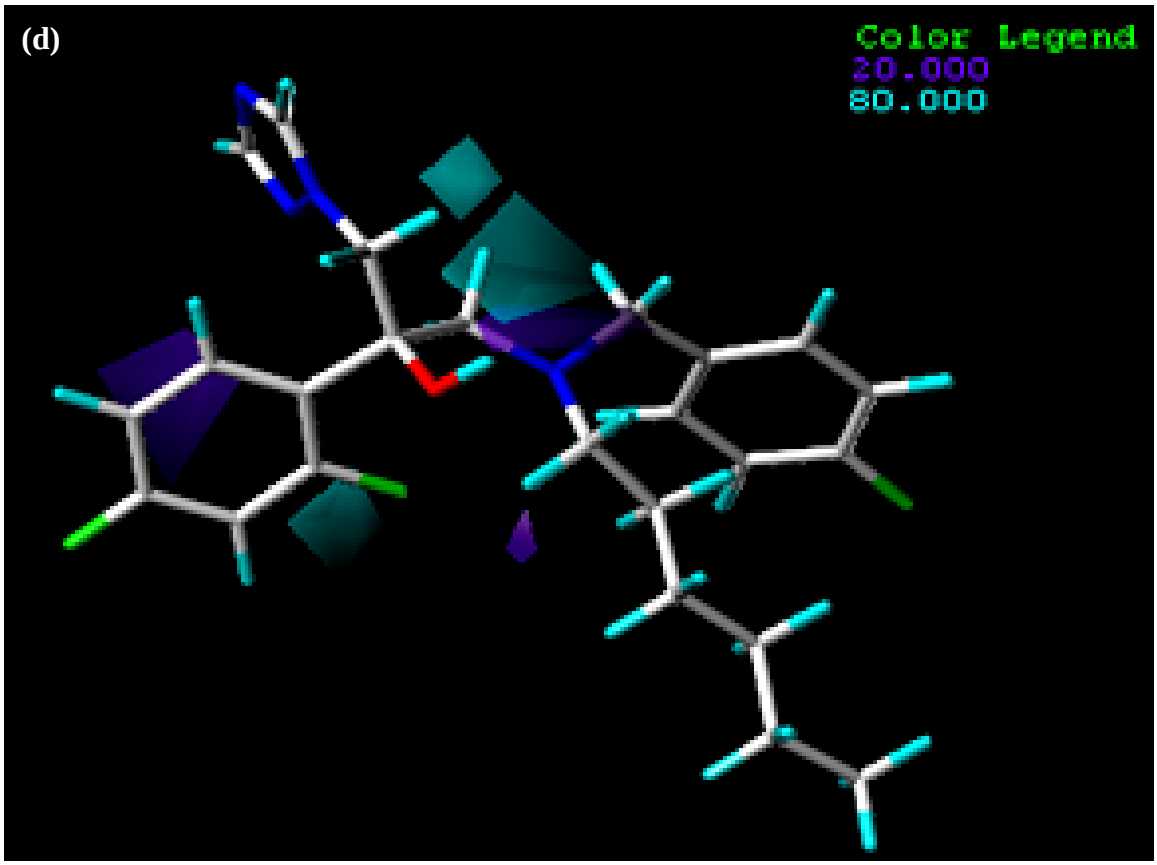
(d)
Color Legend
20.000
80.000

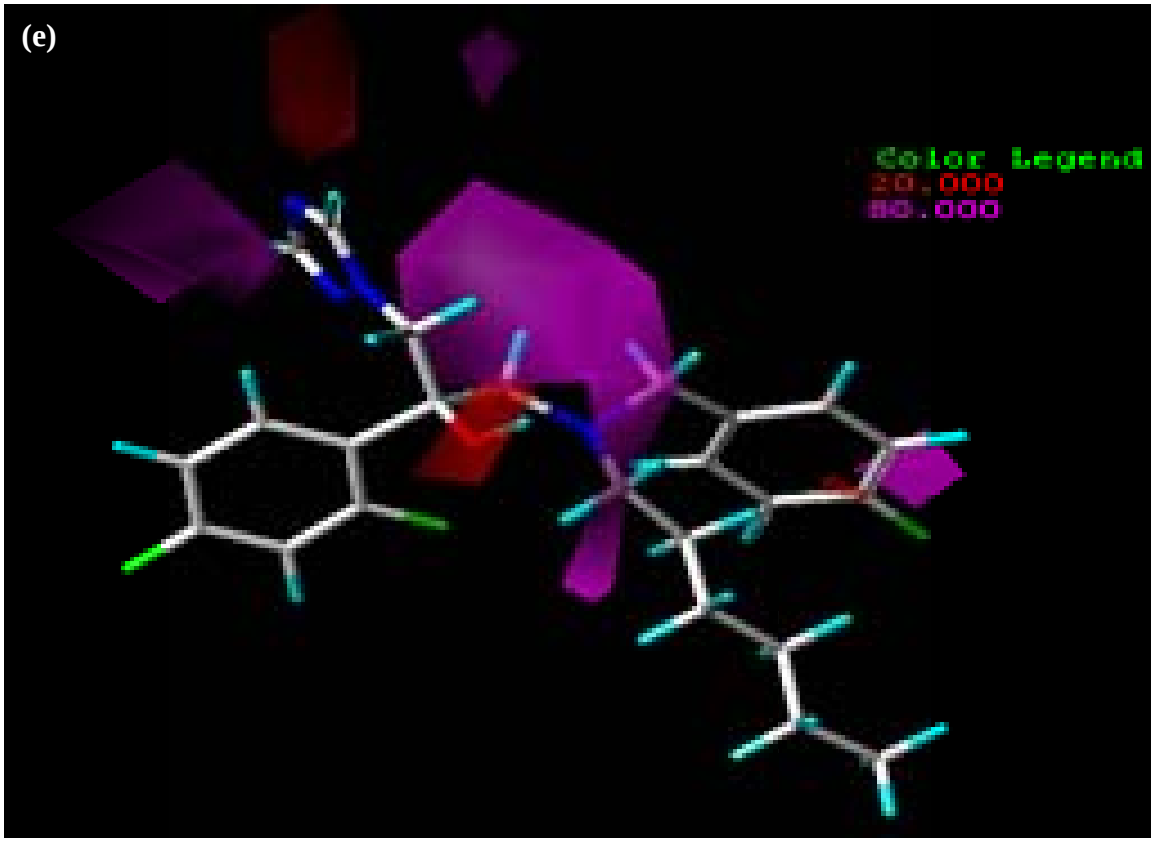
(e)
Color Legend
20.000
80.000

Figure 5.8. Comparative molecular similarity indices analysis (CoMSIA) for least active compound 28(a) Steric map (green, bulky group desirable; yellow, bulky group not desirable),(b) electrostatic map contour map (blue, electropositive group desirable; red, electronegative group desirable), (c) hydrophobic map (yellow, hydrophobic group desirable; white, hydrophilic group desirable), (d) donor map (cyan, donor group desirable; purple, donor group undesirable and (e) acceptor map (magenta, acceptor group desirable; red, acceptor group undesirable).

5.4.4 Docking

To examine the interaction between compounds and Lanosterol 14α-demethylase (CYP51) Docking study was performed. Information obtained by docking study was further utilized for structure modification. Glide was used to perform docking study. Results obtained throw docking of most active inhibitor 8 with CYP51 are shown in Figure 5.9 and 5.10 respectively. For compound 8 Glide docking score was found to be -8.6432. From the interaction with CYP51, it was found that the 2, 4 diflurobenzyl group would generate ∏ - ∏ stacking interaction with PHE 78 and TYR 76 at the hydrophobic clamp. Also, the triazole ring system binds to the heme group which leads to potent antifungal activity.

For the least active compound 28 docking score of for was found to be -7.6200. By analysis of figure 5.11 and 5.12, it is clear that the least active compound 28 does not interact with heme residue. It has a bulky and hydrophobic group at N atom substituent which leads to decrease in the antifungal activity.

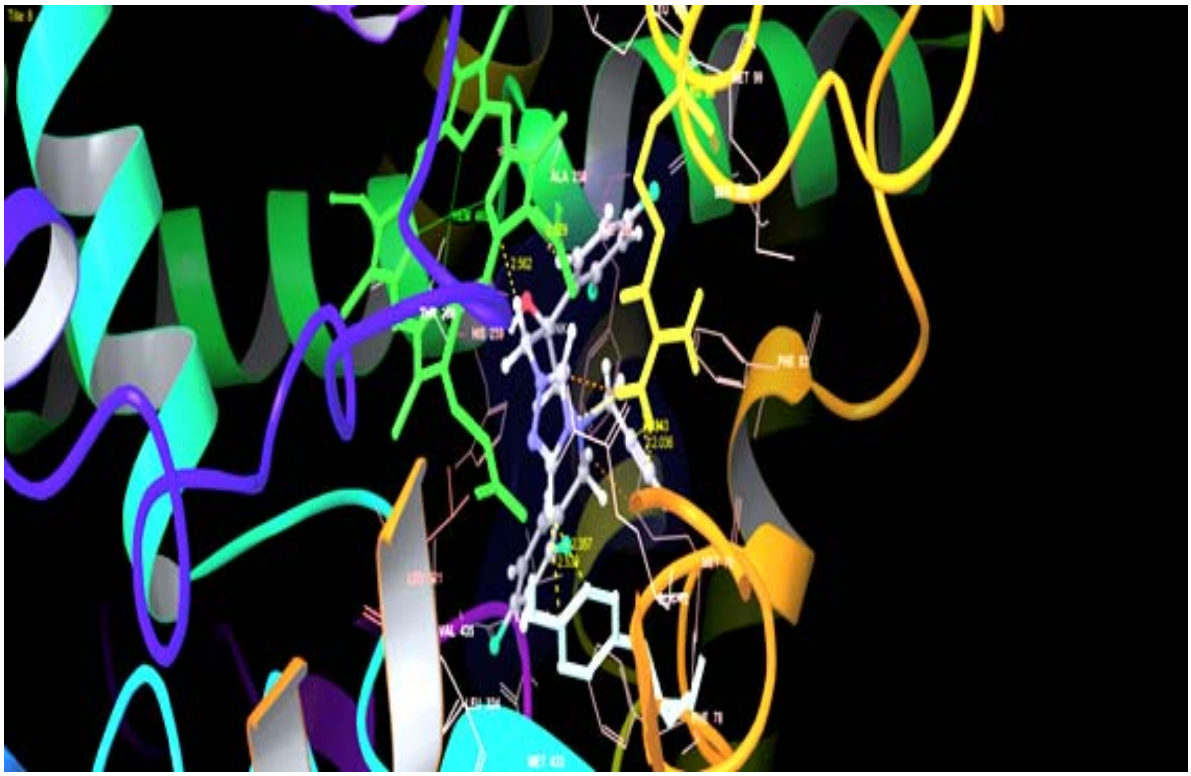

Figure 5.9. Most active compound 8 dockedwith CYP51.

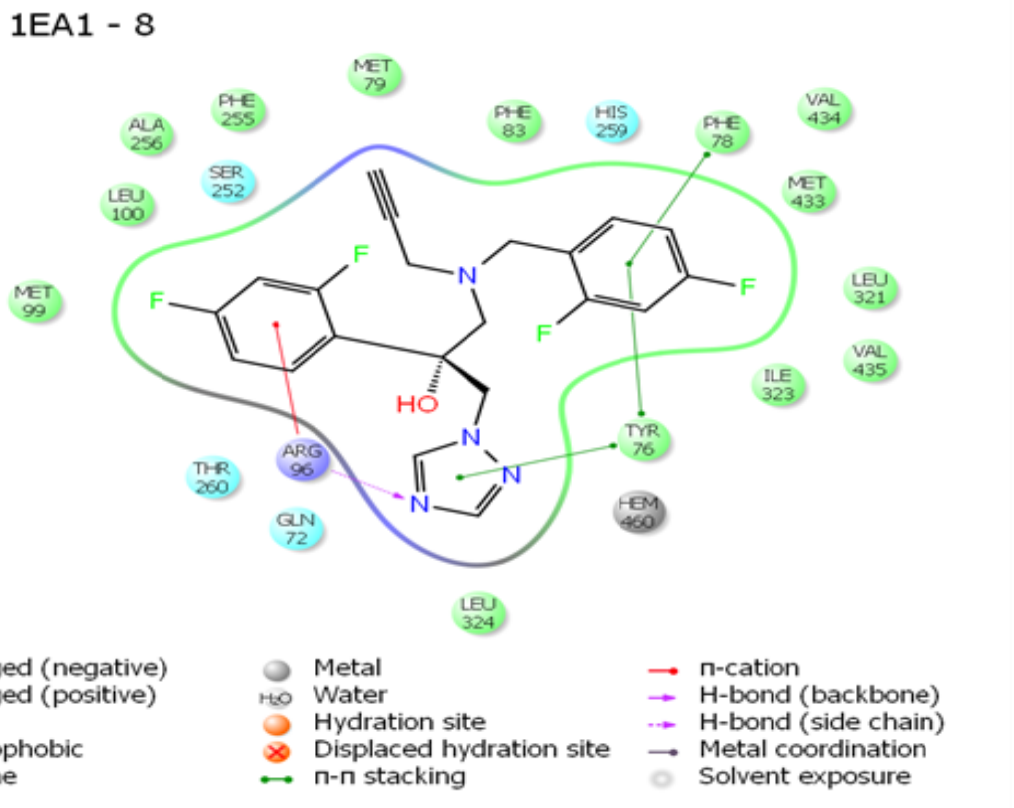

Figure 5.10. 2D view most active compound 8 docked with the active site of CYP51.

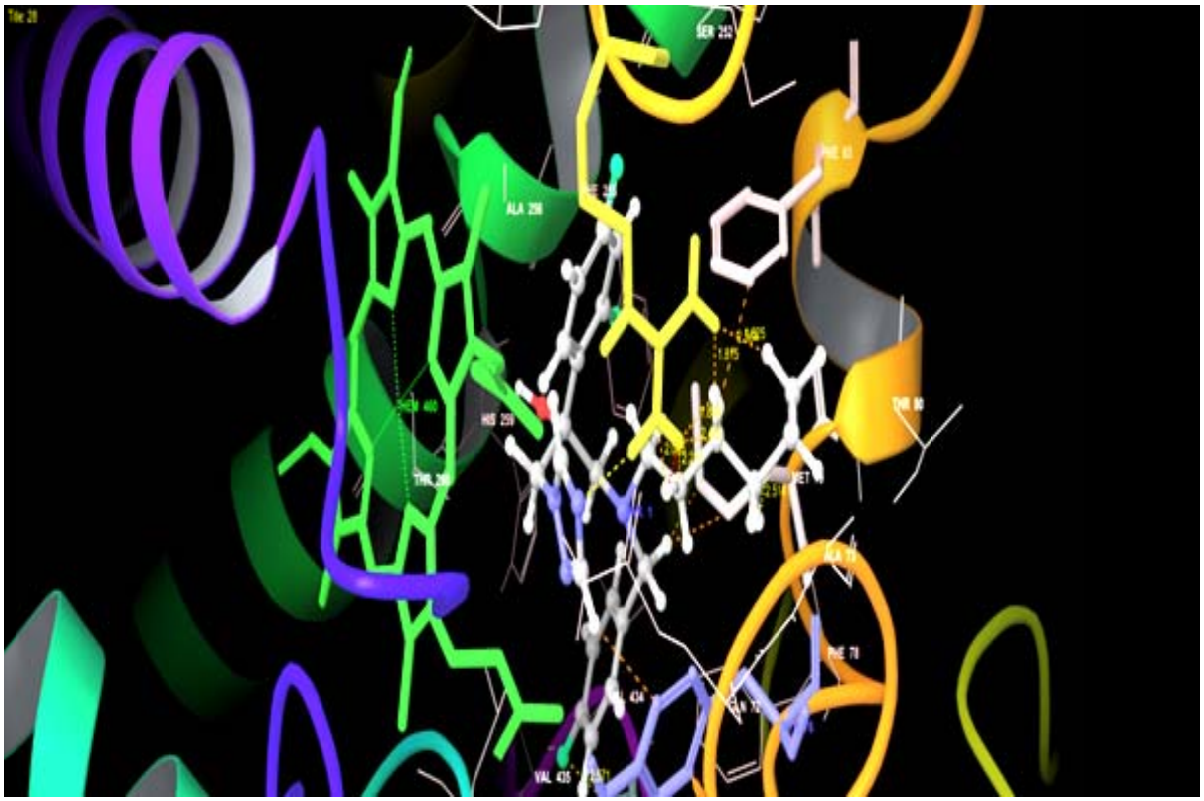

Figure 5.11. Inactive compound 28 docked withCYP51.

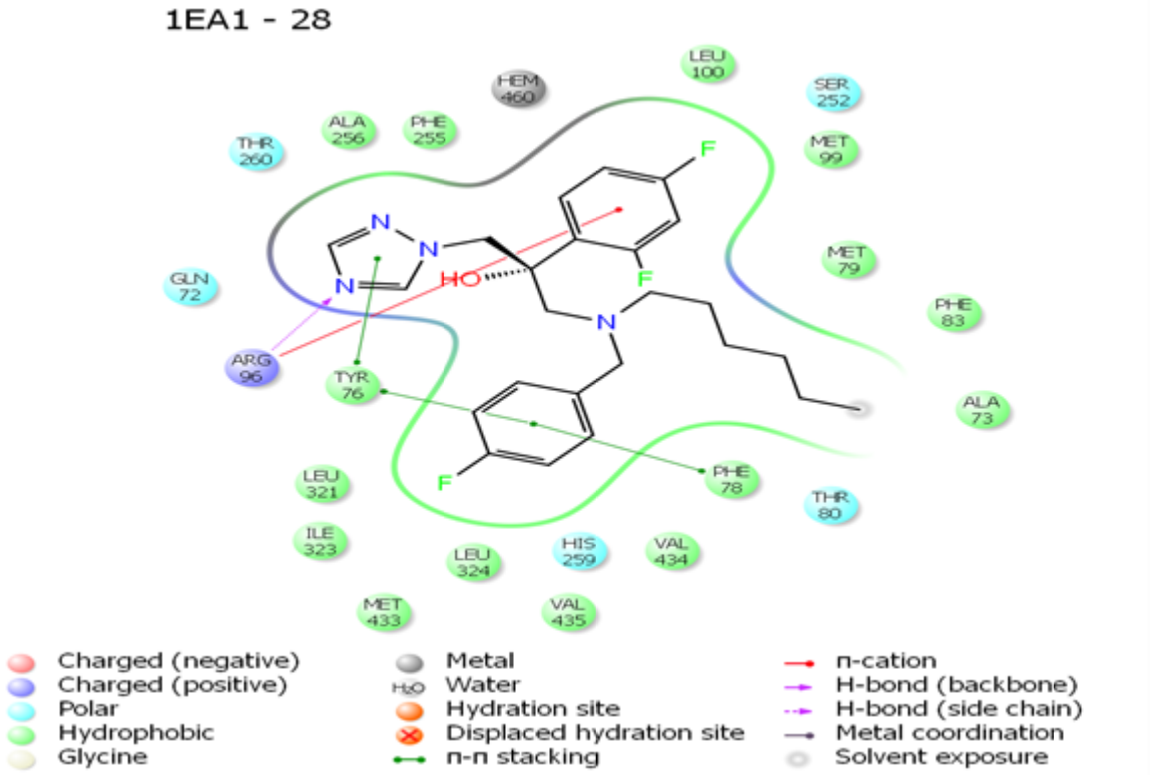

Figure 5.12. 2D view of inactive compound 28 docked with active site of CYP51.

5.5 Conclusion

In the current study, Dataset of lanosterol 14α–demethylase inhibitors utilized to perform CoMFA and CoMSIA study. Partial Least Square (PLS) study was carried out to associate the CoMFA and CoMSIA descriptors with the actual inhibitory activity. The effective 3D-QSAR model was created. Various statistical parameters calculated to validate the created model, and it has found an excellent predictability. The model generated from CoMFA and CoMSIA had the values $q^2 = 0.611$, $r^2_{ncv} = 0.982$, ONC = 5; $q^2 = 0.792$, $r^2_{ncv} = 0.953$, ONC = 5 respectively. Using test set of nine compounds the model was validated. The predictive power of the model was found to be the values of r^2_{pred} as 0.871 and 0.752 of CoMFA and CoMSIA respectively. The boot-strapping analysis was performed to check the robustness and statistical confidence of the derived models. A molecular docking study reveals that most active compound 8 interact with heme group; further, it suggested that bulky group at N atom produces the significant effect on antifungal activity. Whereas, the contour map analysis from CoMFA and CoMSIA model it was observed bulky group is favored at **A** and **C** region but not favored at N atom substituent at **B** region. Hydrogen bond acceptor group as a substituent at triazole ring system leads to increase in the inhibitory activity. Although the CoMFA and CoMSIA models can be utilized further to design novel triazole derivatives as the potent antifungal agent.

5.6 References

[1] Georgopapadakou NH, Walsh TJ. Antifungal agents: chemotherapeutic targets and immunologic strategies. Antimicrobial agents and chemotherapy. 1996; 40: 279-291.

[2] Fridkin SK, Jarvis WR. Epidemiology of nosocomial fungal infections. Clinical microbiology reviews. 1996; 9: 499–511.

[3] Kullberg BJ, Oude LAM. Epidemiology of opportunistic invasive mycoses. European journal of medical research 2002; 7: 183–191.

[4] Enoch DA, Ludlam HA, Brown NM. Invasive fungal infections: a review of epidemiology and management options. Journal of medical microbiology. 2006; 55: 809–818.

[5] Finkelstein E, Amichai B, Grunwald MH. Griseofulvin and its uses. International journal of antimicrobial agents. 1996; 6: 189–194.

[6] Rando RR. Polyenes and vision. Chemistry & biology. 1996; 3: 255–262.

[7] Nailor MD, Sobel JD. Progress in antifungal therapy: Echinocandins versus azoles. Drug Discovery Today: Therapeutic Strategies. 2006; 3: 221-226.

[8] Kauffman CA, Carver PL. Use of azoles for systemic antifungal therapy. Advances in pharmacology. 1997; 39: 143-189.

[9] Birnbaum JE. Pharmacology of the allylamines. Journal of the American Academy of Dermatology. 1990; 23: 782-785.

[10] Wise GJ, Wainstein S, Goldberg P, Kozinn PJ. Flucytosine in urinary Candida infections. Urology. 1974; 3: 708-711.

[11] Odds FC, Brown AJ, Gow NA. Antifungal agents: mechanisms of action. Trends in microbiology. 2003; 11: 272-279.

[12] Sheehan DJ, Hitchcock CA, Sibley CM. Current and emerging azole antifungal agents. Clinical microbiology reviews. 1999; 12: 40-79.

[13] Asai K, Tsuchimori N, Okonogi K, Perfect JR, Gotoh O, Yoshida Y. Formation of azole-resistant Candida albicans by mutation of sterol 14-demethylase P450. Antimicrobial agents and chemotherapy. 1999; 43: 1163-1169.

[14] Bossche HV. Biochemical targets for antifungal azole derivatives: hypothesis on the mode of action. InCurrent topics in medical mycology 1985; 1: 313-351 Springer New York.

[15] Thompson GR, Cadena J, Patterson TF. Overview of antifungal agents. Clinics in chest medicine. 2009; 30: 203-215.

[16] Rodriguez-Fernandez E, Manzano JL, Benito JJ, Hermosa R, Monte E, Criado JJ. Thiourea, triazole and thiadiazine compounds and their metal complexes as antifungal agents. Journal of inorganic biochemistry. 2005; 99: 1558-1572.

[17] Hof H. Is there a serious risk of resistance development to azoles among fungi due to the widespread use and long-term application of azole antifungals in medicine?. Drug resistance updates. 2008; 11: 25-31.

[18] Eggimann P, Garbino J, Pittet D. Management of Candida species infections in critically ill patients. The Lancet infectious diseases. 2003; 3: 772-785.

[19] Pemán J, Cantón E, Espinel-Ingroff A. Antifungal drug resistance mechanisms. Expert review of anti-infective therapy. 2009; 7: 453-460.

[20] Gupta AK, Tomas E. New antifungal agents. Dermatologic clinics. 2003; 21: 565-576.

[21] Lupetti A, Danesi R, Campa M, Del Tacca M, Kelly S. Molecular basis of resistance to azole antifungals. Trends in molecular medicine. 2002; 8: 76-81.

[22] Chai X, Zhang J, Hu H, Yu S, Sun Q, Dan Z, Jiang Y, Wu Q. Design, synthesis, and biological evaluation of novel triazole derivatives as inhibitors of cytochrome P450 14α-demethylase. European Journal of medicinal chemistry. 2009; 44: 1913-1920.

[23] Robbins N, Collins C, Morhayim J, Cowen LE. Metabolic control of antifungal drug resistance. Fungal Genetics and Biology. 2010; 47: 81-93.

[24] Verweij PE, Howard SJ, Melchers WJ, Denning DW. Azole-resistance in Aspergillus: proposed nomenclature and breakpoints. Drug Resistance Updates. 2009; 12: 141-147.

[25] Xiao L, Madison V, Chau AS, Loebenberg D, Palermo RE, McNicholas PM. Three-dimensional models of wild-type and mutated forms of cytochrome P450 14α-sterol demethylases from Aspergillus fumigatus and Candida albicans provide insights into posaconazole binding. Antimicrobial agents and chemotherapy. 2004; 48: 568-574.

[26] De Groot MJ, Ekins S. Pharmacophore modeling of cytochromes P450. Advanced drug delivery reviews. 2002; 54: 367-383.

[27] Tafi A, Anastassopoulou J, Theophanides T, Botta M, Corelli F, Massa S, Artico M, Costi R, Di Santo R, Ragno R. Molecular Modeling of Azole Antifungal Agents Active against Candida albicans. 1. A Comparative Molecular Field Analysis Study 1. Journal of medicinal chemistry. 1996; 39: 1227-1235.

[28] Tafi A, Costi R, Botta M, Di Santo R, Corelli F, Massa S, Ciacci A, Manetti F, Artico M. Antifungal Agents. 10. New Derivatives of 1-[(Aryl)[4-aryl-1 H-pyrrol-3-yl] methyl]-1 H-imidazole, Synthesis, Anti-Candida Activity, and Quantitative Structure-Analysis Relationship Studies. Journal of medicinal chemistry. 2002; 45: 2720-32.

[29] Leemans E, Mahasenan KV, Kumarasiri M, Spink E, Ding D, O'Daniel PI, Boudreau MA, Lastochkin E, Testero SA, Yamaguchi T, Lee M. Three-dimensional QSAR analysis and design of new 1, 2, 4-oxadiazole antibacterials. Bioorganic & medicinal chemistry letters. 2016; 26: 1011-1015.

[30] Tang H, Zheng CH, Ren XH, Liu J, Liu N, Lv JG, Zhu J, Zhou YJ. Synthesis and biological evaluation of novel triazole derivatives as antifungal agents. Chinese Chemical Letters. 2013 Mar 31; 24: 219-222.

[31] Clark M, Cramer RD, Jones DM, Patterson DE, Simeroth PE. Comparative molecular field analysis (CoMFA). 2. Toward its use with 3D-structural databases. Tetrahedron Computer Methodology. 1990; 3: 47-59.

[32] Klebe G, Abraham U, Mietzner T. Molecular similarity indices in a comparative analysis (CoMSIA) of drug molecules to correlate and predict their biological activity. Journal of medicinal chemistry. 1994; 37: 4130-4146.

[33] Cramer RD. Topomer CoMFA: a design methodology for rapid lead optimization. Journal of medicinal chemistry. 2003; 46: 374-388.

[34] Ghasemi JB, Nazarshodeh E, Abedi H. Molecular docking, 2D and 3D-QSAR studies of new indole-based derivatives as HCV-NS5B polymerase inhibitors. Journal of the Iranian Chemical Society. 2015; 12: 1789-1799.

[35] Nazarshodeh E, Shiri F, Ghasemi JB. 3D-QSAR and virtual screening studies in identification of new Rho kinase inhibitors with different scaffolds. Journal of the Iranian Chemical Society. 2015; 12: 1945-1959.

[36] Verma J, Khedkar VM, Coutinho EC. 3D-QSAR in drug design-a review. Current topics in medicinal chemistry. 2010; 10: 95-115.

[37] Bhansali SG, Kulkarni VM. Combined 2D and 3D-QSAR, molecular modelling and docking studies of pyrazolodiazepinones as novel phosphodiesterase 2 inhibitors. SAR and QSAR in Environmental Research. 2014; 25: 905-937.

[38] Rarey M, Kramer B, Lengauer T, Klebe G. A fast flexible docking method using an incremental construction algorithm. Journal of molecular biology. 1996; 261: 470-489.

39. SYBYL-X 1.3 Molecular Modeling Software, Tripos Associates Inc, St. Louis, USA, 2012.

[40] Singla RK, Bhat G V. QSAR model for predicting the fungicidal action of 1, 2, 4-triazole derivatives against Candida albicans. Journal of enzyme inhibition and medicinal chemistry. 2010; 25: 696-701.

[41] Clark M, Cramer RD, Van Opdenbosch N. Validation of the general purpose Tripos 5.2 force field. Journal of Computational Chemistry. 1989; 10: 982-1012.

[42] Purushottamachar P, Kulkarni VM. 3D-QSAR of N-myristoyltransferase inhibiting antifungal agents by CoMFA and CoMSIA methods. Bioorganic & medicinal chemistry. 2003; 11: 3487-3497.

[43] Böhm M, Stürzebecher J, Klebe G. Three-dimensional quantitative structure-activity relationship analyses using comparative molecular field analysis and comparative molecular similarity indices analysis to elucidate selectivity differences of inhibitors binding to trypsin, thrombin, and factor Xa. Journal of medicinal chemistry. 1999; 42: 458-477.

[44] Golbraikh A, Tropsha A. Beware of q 2!. Journal of Molecular Graphics and Modelling. 2002; 20: 269-276.

[45] Glide, version 5.8, Schrödinger LLC, New York, NY, 2012.

[46] Friesner RA, Banks JL, Murphy RB, Halgren TA, Klicic JJ, Mainz DT, Repasky MP, Knoll EH, Shelley M, Perry JK, Shaw DE. Glide: a new approach for rapid, accurate docking and scoring. 1. Method and assessment of docking accuracy. Journal of medicinal chemistry. 2004; 47: 1739-1749.

[47] Halgren TA, Murphy RB, Friesner RA, Beard HS, Frye LL, Pollard WT, Banks JL. Glide: a new approach for rapid, accurate docking and scoring. 2. Enrichment factors in database screening. Journal of medicinal chemistry. 2004; 47: 1750-1759.

[48] Maestro, version 9.3, Schrödinger LLC, New York, NY, 2012.

[49] LigPrep, version 2.5, Schrödinger LLC, New York, NY, 2012.

[50] Chang G, Guida WC, Still WC. An internal-coordinate Monte Carlo method for searching conformational space. Journal of the American Chemical Society. 1989; 111: 4379-4386.

[51] Kolossváry I, Guida WC. Low mode search. An efficient, automated computational method for conformational analysis: Application to cyclic and acyclic alkanes and cyclic peptides. Journal of the American Chemical Society. 1996; 118: 5011-5019.